Available online at www.sciencedirect.com

ScienceDirect

Journal of Magnesium and Alloys 11 (2023) 2833–2852

www.elsevier.com/locate/jma

Full Length Article

Effect of Cd on matrix structure ordering and aging precipitation evolution in a Mg-Gd-Cd solid-solution alloy

Lin-Lin Liu, Wei Sun*, Cuixiu Liu, Pengyang Sun

Institute of Microstructure and Property of Advanced Materials, Beijing University of Technology, Beijing 100124, China

Received 2 February 2021; received in revised form 19 October 2021; accepted 21 October 2021
Available online 6 December 2021

Abstract

The formation and evolution of Gd-rich precipitates companying with the matrix structure ordering in a $Mg_{97}Gd_2Cd_1$ (at.%) solid-solution alloy aged at 200 °C have been systemically investigated using high-angle annular dark-field scanning transmission electron microscopy (HAADF-STEM). The results show that Gd-rich precipitation dynamics during the aging treatment are noticeably affected by a continuous ordering transformation in the matrix. The ordering transformation process involving mainly re-distribution of Cd atoms was revealed to occur in the following way: random super-saturated solid solution (S.S.S.S.) → $B19$-type ordered domains → $D0_{19}$-type ordered domains. Four Gd(Cd)-rich precipitates, G.P. I zone, G.P. II zone, β' and β_1 phases, have been observed to be formed in sequence to coexist with the various ordered domains. Based on the HAADF-STEM characterization on the aging microstructures at different aging stages, it can be concluded that the Cd-addition and related matrix structure ordering can play significant roles in modifying the early-stage G.P. zone structure, altering the morphology of β' precipitates and promoting the forming ability of the β_1 precipitate.

Keywords: Mg-Gd-Cd alloy; Ordering transformation; Aging microstructure; Precipitation evolution; HAADF-STEM.

1. Introduction

Magnesium rare-earth (Mg-RE) alloys are of a critical class of lightweight metal structural materials that have been studied for more than a decade [1–3]. Compared with other Mg alloys, Mg-RE alloys exhibit excellent resistance to corrosion and high-temperature creep, and thus have broad application prospects in the fields of industry, transportation, aerospace and electronic communication [3–9]. It has been well documented that superior mechanical properties for Mg-RE alloys can be achieved through precipitating various dispersed nano-sized RE-rich strengthening phases in the Mg matrix [2,10-18]. Obviously, exploring precipitation varieties and figuring out more effective factors for controlling the formation and evolution of RE-rich precipitates are of great significance for developing multipurpose Mg alloys.

For achieving desirous precipitation microstructures so as to improve the general performance of binary Mg-RE alloys, adding a third kind of alloying element and performing appropriate heat treatments had been proved to be highly feasible means for this goal. It had been widely reported that the addition of RE elements of different kinds or adding transition group elements of different groups can effectively regulate the strengthening precipitation microstructure through altering the precipitation dynamics, precipitate morphology and distribution in the Mg alloy matrix. For instance, for binary Mg-Y and Mg-Gd alloys in which the β_1 precipitation phase is rarely formed during the conventional aging treatment at 200 – 250 °C, the addition of Nd or Sm to these two alloys can promote the β_1-phase precipitation such that the precipitated β_1-phases of high-density can connect alternately with the coexisting β'-phases to form characteristic long chains or network extensively [11–18]. Also, adding Zn or Al, Ag, Co, Cu and Ni to binary Mg-RE alloys instead of adding other different kinds of RE elements can induce the formation of layered G.P. zones, γ'''-, γ''-, γ'-, γ-phases, or LPSO-phases,

* Corresponding author.
E-mail address: weisun@bjut.edu.cn (W. Sun).

https://doi.org/10.1016/j.jma.2021.10.012

in the corresponding Mg alloy matrix along the basal plane [19–31]. In essence, the precipitation diversity in Mg-RE alloys, as mentioned above, is mainly due to the fact that the added alloying elements can directly involve in the formation of various precipitates, exhibiting different bonding and electronic structure features [32–35]. On the other hand, in view of the fact that solid-solution strengthening of alloy matrix is also an effective strengthening means for Mg-RE alloys, one can consider adding a certain kind of alloying elements that can mainly act as a solid solute in the alloy matrix rather than contribute itself mostly to precipitation phase formation. It is believed that a solid-soluted Mg alloy can be further strengthened when allowing an ordering transformation to occur in its matrix since the motion of deformation dislocations under stress is more difficult in an ordered matrix structure than in its random counterpart [36–38].

According to the Mg-based binary phase diagrams, Cd is the only alloying element being capable of dissolving in any ratio into the Mg matrix to form a complete solid solution at a certain temperature [39,40]. Unlike the above-mentioned alloying elements, which can directly contribute to precipitation phase formation, the Cd element has been considered for other purposes. It has been reported that the addition of Cd to some Mg alloys could play an effective role in improving their anti-corrosion properties and refining their grain size [41–45]. However, less attention has been paid to its possible influence on the RE-rich precipitation evolution in an age-hardenable Mg-RE alloy so far. Only quite recently, it has been reported that adding Cd to Mg-Sm alloy can effectively enhance aging-hardening response due to Sm/Cd-rich precipitation at the early aging stage [46], however its effects on the precipitation evolution and matrix structure ordering are not mentioned. For the Mg-Cd binary system, element Cd can have infinite solid solubility in Mg when the temperature is above 253 °C [40]. In contrast to those aged Mg-RE alloys with complex precipitation structures, the Mg-Cd alloy system subjected to the same aging treatment should be much simple in phase constitution and related aging microstructure. A remarkable feature of phase transformation in the Mg-Cd alloy system is that the ordered $Mg_3Cd/MgCd_3$ and MgCd phases which have $D0_{19}$ and B_{19} structures respectively can be formed within a wide composition ranges at temperatures lower than 253 °C [40]. In view of the alloying effect of Cd in Mg, it is expectable that adding Cd to an age-hardenable Mg-RE alloy shall introduce a microstructure controlling factor relevant to the Cd-atom ordering in the Mg matrix, through which an ordered matrix diverged from the random solid solution one could be developed for the RE-rich phase precipitation. This consideration can be taken as a possible strategy for exploring a new approach to diversify precipitation structures, which could allow mechanical and anti-corrosion performances of Mg-RE alloys to be adjusted more flexibly and comprehensively. However, what type of ordered matrix can actually be formed in a Mg-RE-Cd alloy and what is its formation process? What are the effects of Cd-addition and related ordering process as well as ordered structure in the matrix on the RE-rich precipitation behaviors and precipitate structures? Can the combination of the matrix structure ordering and the RE-rich precipitation really cause new or characteristic aging microstructures? These are still open questions without definite answer so far.

In the present study, we have developed an age-hardening Mg-Gd-Cd alloy in which Gd-rich strengthening phases can be precipitated under the influence of the ordering transformation in the α-Mg matrix during aging treatments. High-angle annular dark-field scanning transmission electron microscopy (HAADF-STEM) technique has been applied to examine the microstructural evolutions involved with the ordering transformation and concurrent Gd-rich precipitation in the alloy matrix during the aging treatment at 200 °C. Our objectives are to provide reliable HAADF-STEM characterization results relevant to the aging microstructures at different aging stages for the Mg-Gd-Cd alloy. On the basis of these, we try to clarify the effects of Cd on the matrix structure ordering and the Gd-rich precipitation, and further to ascertain the relevant evolution characteristics and mechanisms.

2. Experimental procedures

An alloy ingot with a nominal composition of $Mg_{97}Gd_2Cd_1$ (at.%) and a weight of about 10 gs was prepared by melting high-purity (>99.99%) Mg, Gd, and Cd in a high-frequency induction furnace under the protection of pure argon gas. The as-cast ingot was then divided into small parts for the subsequent experiment. The actual chemical composition of the obtained alloy was determined to be $Mg_{96.8}Gd_{2.1}Cd_{1.1}$ (at.%) by using an X-ray fluorescence spectrum analyzer (Magix PW2403). Similarly, a $Mg_{98}Gd_2$ (at.%) alloy ingot (measured composition: $Mg_{97.8}Gd_{2.2}$ (at.%)) was also prepared subsequently as a binary alloy reference for the hardness testing and aging microstructural characterization. The as-cast samples, sealed in evacuated quartz tubes, were solution-treated at 530 °C for 10 h and then quenched into water. The aging treatments for the as-quenched samples were carried out at 200 °C for different periods of time. Vickers hardness testing for the aged alloy samples was performed using a hardness tester (HMV-1T) with a load of 100 gs and a dwell time of 10 s. Transmission electron microscope (TEM) specimens were prepared by twin jet electro-polishing at −20 °C in a solution with 15% nitric acid, 15% glycerol and 70% methanol, using a Struers Tenupol-5 electro-polisher, and subsequently low-energy ion thinning was carried out in order to clean the specimen surfaces. HAADF-STEM characterizations of the precipitation structures at different aging stages were carried out using an FEI Tecnai G^2 F20 TEM operated at 200 kV as well as an FEI Titan G^2 60–300 TEM equipped with a probe Cs corrector and operated at 300 kV. The HAADF-STEM images were acquired with a collection angle in the range of 76 – 200 mrad. EDS element mapping was performed using an FEI super-X EDS detector system attached to the FEI Titan G^2 60–300 TEM. Furthermore, quantitative EDS chemical composition analysis for any selected region was realizable through calculating its average element content from the obtained element mapping data.

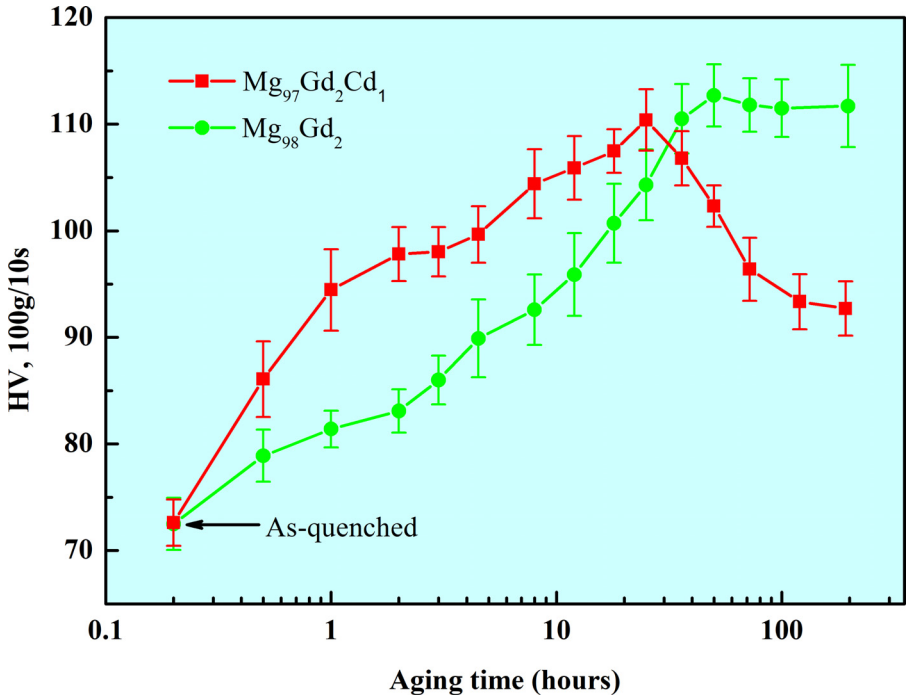

Fig. 1. Aging hardening response of the $Mg_{97}Gd_2Cd_1$ (at.%) alloy aged at 200 °C, presented together with that of the aged $Mg_{98}Gd_2$ (at.%) alloy for comparison.

3. Results

3.1. Age-hardening response of the Mg-Gd-Cd alloy

In order to reveal the age-hardening behavior of the $Mg_{97}Gd_2Cd_1$ alloy, hardness testing was carried out after the as-quenched samples were aged at 200 °C. The typical hardening response with the aging time at 200 °C is shown in Fig. 1, from which one can see that the hardness increases continuously from an initial of ~72 HV to a peak value of ~110 HV after the as-quenched sample was aged at 200 °C for 25 h. For comparison, the aging hardening response for a binary $Mg_{98}Gd_2$ alloy aged at 200 °C is also presented in Fig. 1 (see the green curve). It is obvious that the aging hardening response for the solution-treated $Mg_{97}Gd_2Cd_1$ alloy at 200 °C is quite swift at early aging stage, since its hardness value is higher and can increase more rapidly compared with the case for the aged $Mg_{98}Gd_2$ alloy. More specifically, for the Mg-Gd-Cd sample aged at 200 °C for 2 h, its hardness value (~97 HV) had already reached to about 88% of the peak value (~110 HV), while for the Mg-Gd sample subjected to the same aging treatment, its hardness value (~83 HV) is just about 73% of the peak value (~113 HV). Accordingly, it can be said that the aging hardening process in the Mg-Gd-Cd system tends to be accelerated due to the Cd-addition. Notice that there exists a small plateau (or a shoulder) ranging roughly from $t = 2$ to 4 h in the hardness curve for the $Mg_{97}Gd_2Cd_1$ alloy, indicating that the hardening rate appears to have a brief slowdown before increase again to achieve the peak value of hardness at 25 h. With further increase of the aging time, the hardness value will decrease from the peak, and then gradually sustains at ~92 HV when the aging time exceeds about 200 h. Obviously, the $Mg_{97}Gd_2Cd_1$ alloy has a definite age-hardening response when heat-treated at 200 °C and thus belongs to a typical aging-hardenable alloy. Notice that, in comparison with the peak-hardness value of the aged $Mg_{98}Gd_2$ alloy, that of the aged $Mg_{97}Gd_2Cd_1$ alloy is just slightly lower but does not exhibit a considerable difference.

3.2. Experimental observations of aging microstructures and evolutions

3.2.1. Structure of the Mg-Gd-Cd super-saturated solid solution

A super-saturated solid solution (S.S.S.S.) state for the $Mg_{97}Gd_2Cd_1$ alloy can be established by solution treatment at 530 °C for 10 h, during which the solute-rich primary phases distributed dendritically in the as-cast Mg-Gd-Cd alloy had mostly dissolved into the Mg matrix (see Figs. 2(a, b)). Further solution treatment at 530 °C for an even longer time can no longer bring about any obvious variation in microstructure, indicating that the solid-solution treatment (530 °C + 10 h) is sufficient to allow the alloy matrix to reach a super-saturated state. For the obtained Mg-Gd-Cd S.S.S.S., its matrix structure can be directly revealed through HAADF-STEM observation at atomic-scale resolution. As seen in Fig. 2c, the overall bright-dot-contrast distribution corresponding to the long-range hexagonal arrays of atom pillars in the α-Mg alloy matrix appears to be homogeneous. It is clear that no prominent ordered structure exists in the Mg-Gd-Cd S.S.S.S. alloy matrix except for the presence of a few atomic pillars with slightly brighter contrast in some

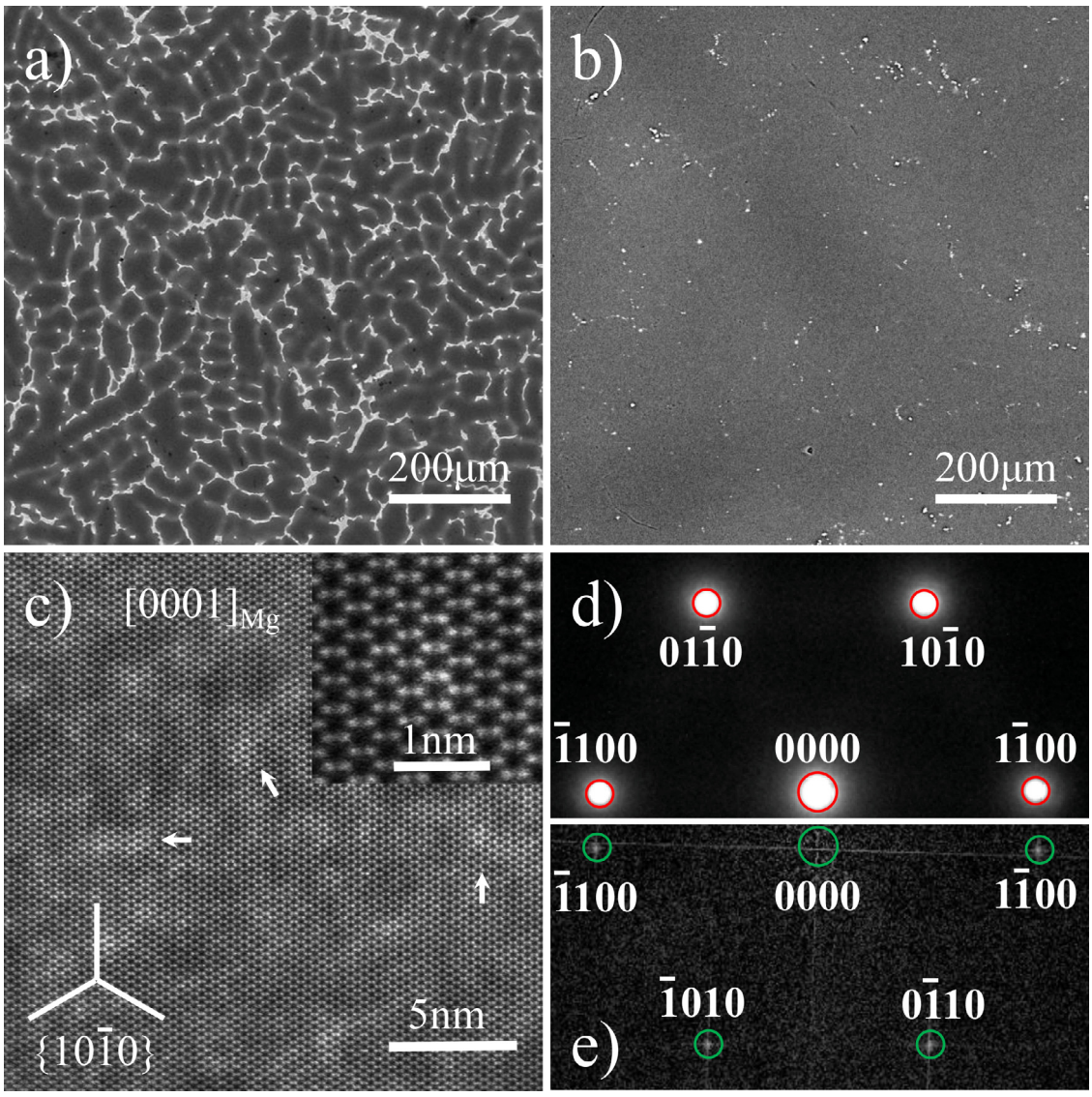

Fig. 2. Backscattered electron images of (a) as-cast and (b) solution-treated $Mg_{97}Gd_2Cd_1$ (at.%) alloys; (c) Atomic-scaled HAADF-STEM image (with an enlarged part being inserted) showing the solution-treated structure of the alloy matrix along the $[0001]_{Mg}$ axis; (d) Selected area electron diffraction (SAED) pattern taken from a region larger than (c); (e) Fast Fourier transform (FFT) pattern corresponding to (c).

local regions. Since the brightness of each atomic pillar in the HAADF-STEM image is roughly proportional to the square of the average atomic number (Z^2) of the constituent elements, the Z-contrast variation for a small group of atomic pillars in some local regions (such as those indicated with arrows in Fig. 2c) can thus be attributed to locally inhomogeneous chemical fluctuations of solute atoms. Figs. 2(d) and 2(e) are two part patterns corresponding respectively to the selected area electron diffraction (SAED) from the solution-treated alloy matrix and the fast Fourier transform (FFT) from the observed HAADF-STEM image. As can be seen from these two patterns, no extra diffraction spot or even diffuse one can be detected to correlate with the presence of any precipitate or local ordered structure. On the whole, it can be regarded that the solute atoms, including Gd with limited solid solubility and Cd with infinite solid solubility in Mg, are distributed randomly in the alloy matrix of the Mg-Gd-Cd super-saturated solid solution.

3.2.2. G.P. I zone segregation and concurrent B_{19}-type ordering in the matrix

For the Mg-Gd-Cd sample aged at 200 °C for 2 h, TEM observation along the $[0001]_{Mg}$ axis clearly revealed that plenty of long thin-plate-like products with an average length of ~20 nm were precipitated densely in the Mg-Gd-Cd matrix along its $\{10\bar{1}0\}_{Mg}$ planes (see Fig. 3a). In the corresponding selected area electron diffraction (SAED) pattern presented in Fig. 3b, long weak streaks caused by those irregularly-spaced platelet precipitates can be seen along each of $< 10\bar{1}0 >_{Mg}^{*}$ directions, as indicated by green arrows. Note also that in Fig. 3b, extra sharp spots (marked with blue circles) appear at 1/2 positions between the transmission and the main

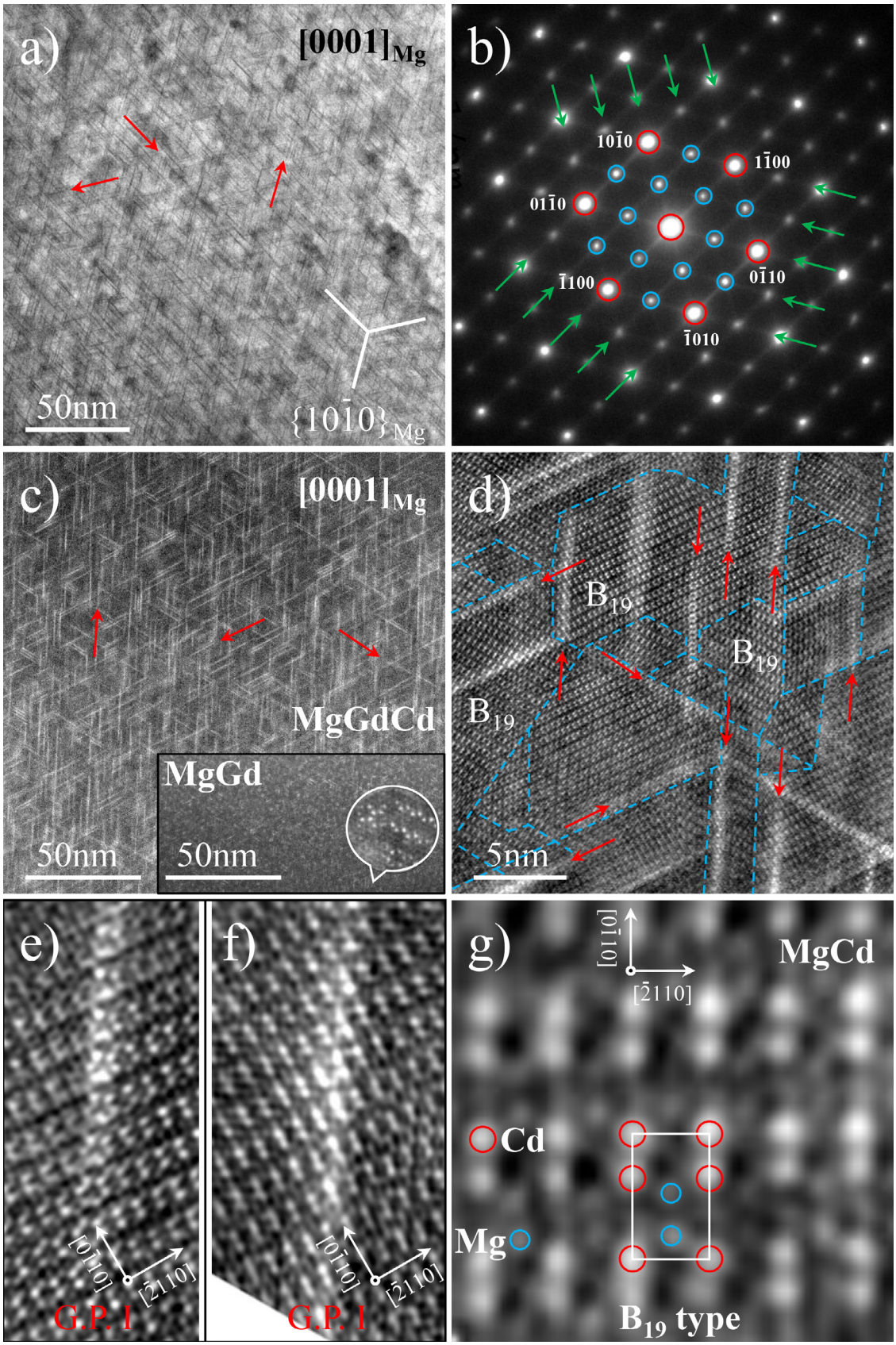

Fig. 3. Structural observation of the $Mg_{97}Gd_2Cd_1$ (at.%) alloy aged at 200 °C for 2 h along the $[0001]_{Mg}$ axis, showing that the G.P. I zones were formed coexisting with B_{19}-type ordered domains. (a) TEM bright-field image; (b) Selected area electron diffraction (SAED) pattern; (c, d) Low- and high-magnification HAADF-STEM images; (e, f) HAADF-STEM images for two typical platelet G.P. I zones; (g) Atomic-scale HAADF-STEM image of the ordered structure of the B_{19}-type. For comparison, a HAADF image taken along the $[0001]_{Mg}$ axis from the $Mg_{98}Gd_2$ (at.%) aged at 200 °C for 2 h is inserted in (c).

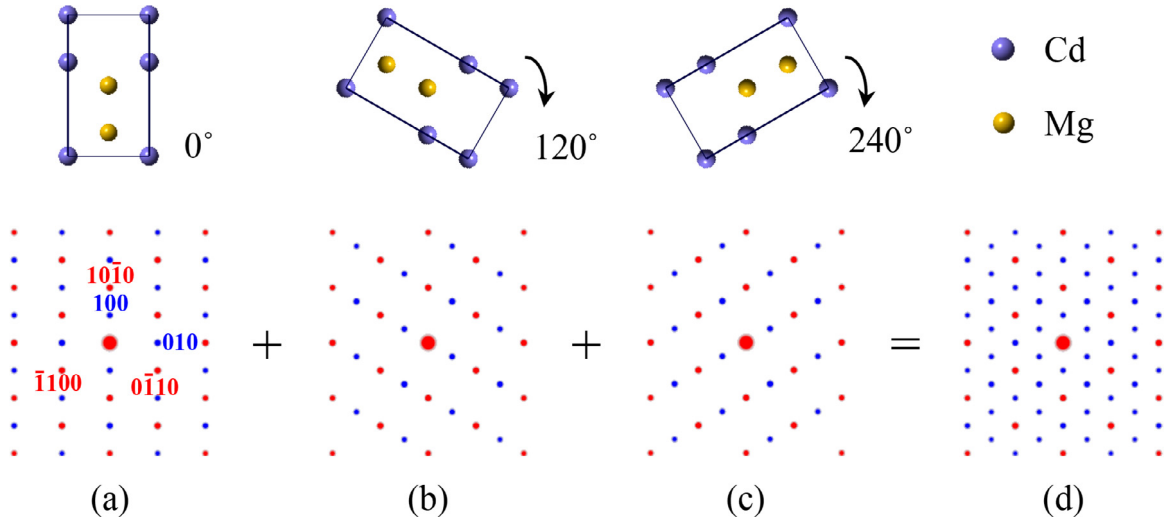

Fig. 4. (a) ∼ (c) Schematic illustration showing the existence of three orientational variants for the B_{19}-type ordered domains formed in the Mg matrix (the first row). The corresponding diffraction patterns along the $[0001]_{Mg}$ direction are given in the second row, where blue and red spots represent diffraction spots from the ordered domains and the Mg matrix, respectively. (d) Overlapping the patterns in (a) ∼ (c) can reproduce the observed hexagonal diffraction pattern as shown in Fig. 3b.

diffraction spots of the α-Mg matrix (outlined with red circles), which indicates that the matrix had initiated an ordering process at this aging stage.

As can be seen in Figs. 3(c, d), the long thin-plate precipitates exhibit significant bright contrasts in HAADF-STEM images, indicating that they are mainly rich in Gd atoms with a large atomic number. Actually, the Cd atoms co-precipitating with Gd atoms also involve in the formation of these long thin-plate precipitates even though the forming process is mainly dominated by the Gd precipitation. This fact can be seen clearly in Fig. 6 where the EDS mapping analysis on the long thin-plate precipitates formed in the early aging stage is presented. It is obvious that those long thin precipitates clearly seen in the HAADF image (see Fig. 6a) can have a much more definite morphology in the Gd-mapping than in the Cd-mapping images (compare Figs. 6c and 6d). Atomic-scale HAADF-STEM observations further revealed that these long thin precipitates were formed with a thickness ranging just 2∼4 atomic layers in the ordered matrix, and the corresponding arrangements of Gd(Cd) atoms in these layers were observed to be only in a less-ordered or less-definite state (see Figs. 3(e, f)). Therefore, as major precipitation products at the early aging stage, these long thin-plate precipitates can be regarded as a kind of G.P. zone of compositional segregation. It will be referred to as G.P. I zone hereinafter.

Companying with the segregation of G.P. I zones, the occurrence of matrix structure ordering had also been revealed by HAADF-STEM observation directly. As can be seen in Fig. 3d, ordered domains with three orientational variants (such as those bounded with blue dashed lines) had been formed coherently in the matrix, whose dimensions were only ∼2 nm to ∼30 nm in average diameter. In each domain, atomic pillars, imaging to exhibit second brightest Z-contrasts for Cd and weak ones for Mg atoms, primarily arrange following a B_{19}-type ordered structure (see Fig. 3g), namely the ordered domains are structurally identical to the B_{19}-type MgCd phase [47]. In fact, it is the existence of these B_{19}-type domains that give rise to the extra sharp diffraction spots in the observed SAED pattern (see those marked with blue circles in Fig. 3b). As schematically illustrated in Fig. 4, the hexagonal distribution of these extra diffraction spots observed in the diffraction pattern of Fig. 3b is a result of multiple diffraction contributions from three orientational domain variants of the B_{19}-type.

3.2.3. G.P. I-to-G.P. II structural transformation and concurrent DO_{19}-type matrix ordering

With the increasing of aging time from 2 to 4 h, the predominant precipitates in the matrix did not exhibit apparent variations in morphology, dimension and distribution density (see Fig. 5a). Nevertheless, in addition to the G.P. I zones of majority (such as those indicated by red arrows in Fig. 5b), a few newly-formed Gd-rich linear precipitates with a definite zigzag feature can be recognized through high-magnification HAADF-STEM observations, such as those indicated by green arrows in Figs. 5(b, c, d). Obviously, unlike the G.P. I zone whose structure is less-definite, this kind of zigzag chain-like Gd-rich precipitate is structurally unambiguous. As clearly revealed in Fig. 5c of an atomic-scaled HAADF-STEM image, each single Gd-rich zigzag chain is structurally consistent with the Gd-rich building layer for constructing the well-known β' phase whose structure is characterized by the stacking of zigzag arrangement rows of RE atoms [13,48-55]. Actually, in the Mg-Gd-Cd alloy aged in such an early stage, the specific stacking configuration consisting of two parallel zigzag chains with a mirror relation and an interval of ∼1.11 nm in the $< 10\bar{1}0 >_{Mg}$ direction had been established in some regions (see Fig. 5d), which can be regarded as a β' nucleus with half-constructed β' structure since only half-β'-unit-cells can be outlined from it. On the

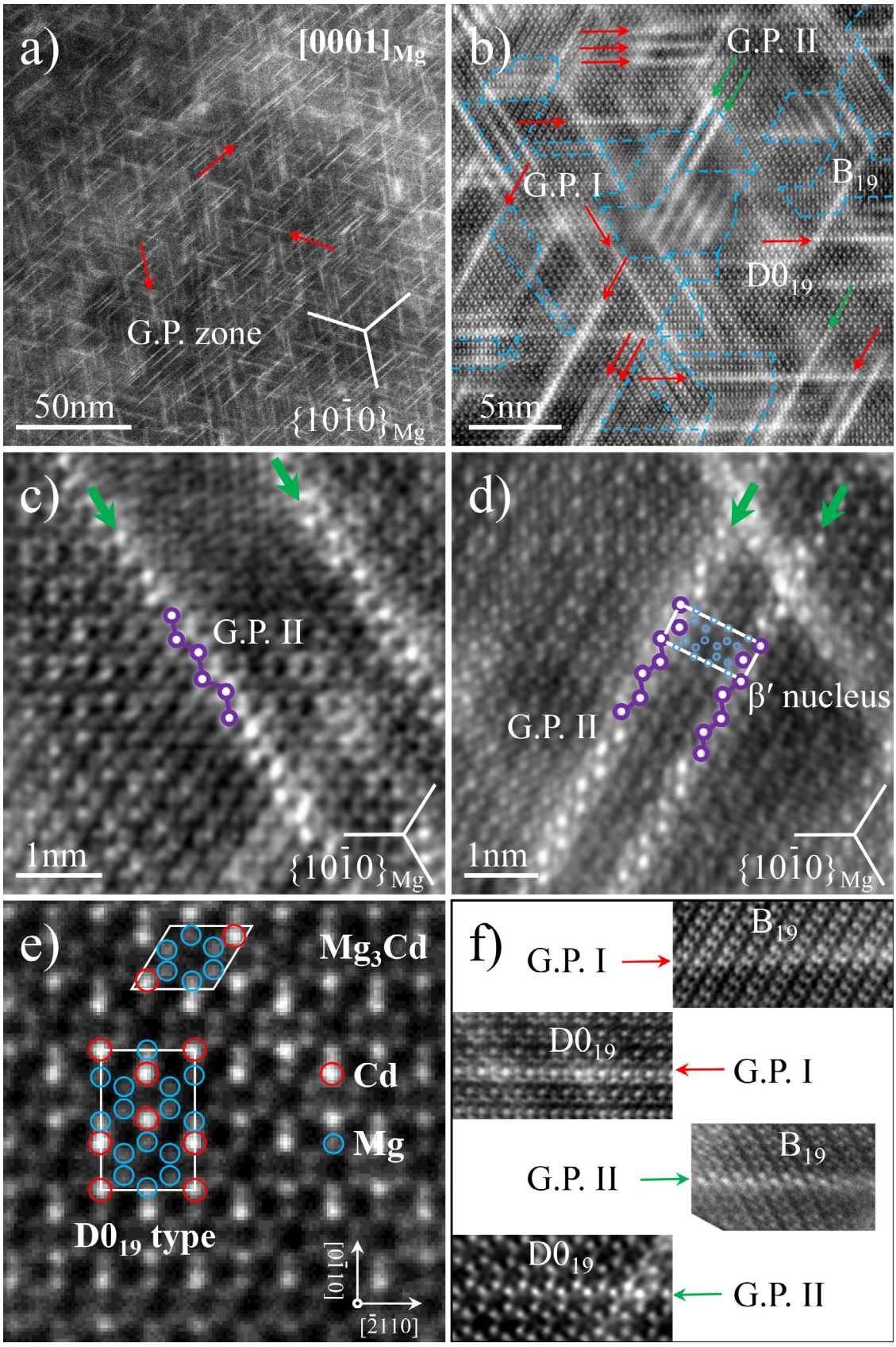

Fig. 5. (a) Low- and (b) high-magnification HAADF-STEM imaging for the $Mg_{97}Gd_2Cd_1$ (at.%) alloy aged at 200 °C for 4 h along its $[0001]_{Mg}$ axis; Atomic-scaled HAADF-STEM images showing (c) zigzag chain-like G.P. II zones in the ordered matrix and (d) characteristic stacking of two zigzag G.P. II zones which can be regarded as a β' nucleus with half-constructed β' structure; (e) Atomic-scaled HAADF-STEM image of the $D0_{19}$-type ordered structure; (f) HAADF-STEM images showing that G.P. I and G.P. II zones can exist in B_{19}-type and $D0_{19}$-type ordered domains, respectively.

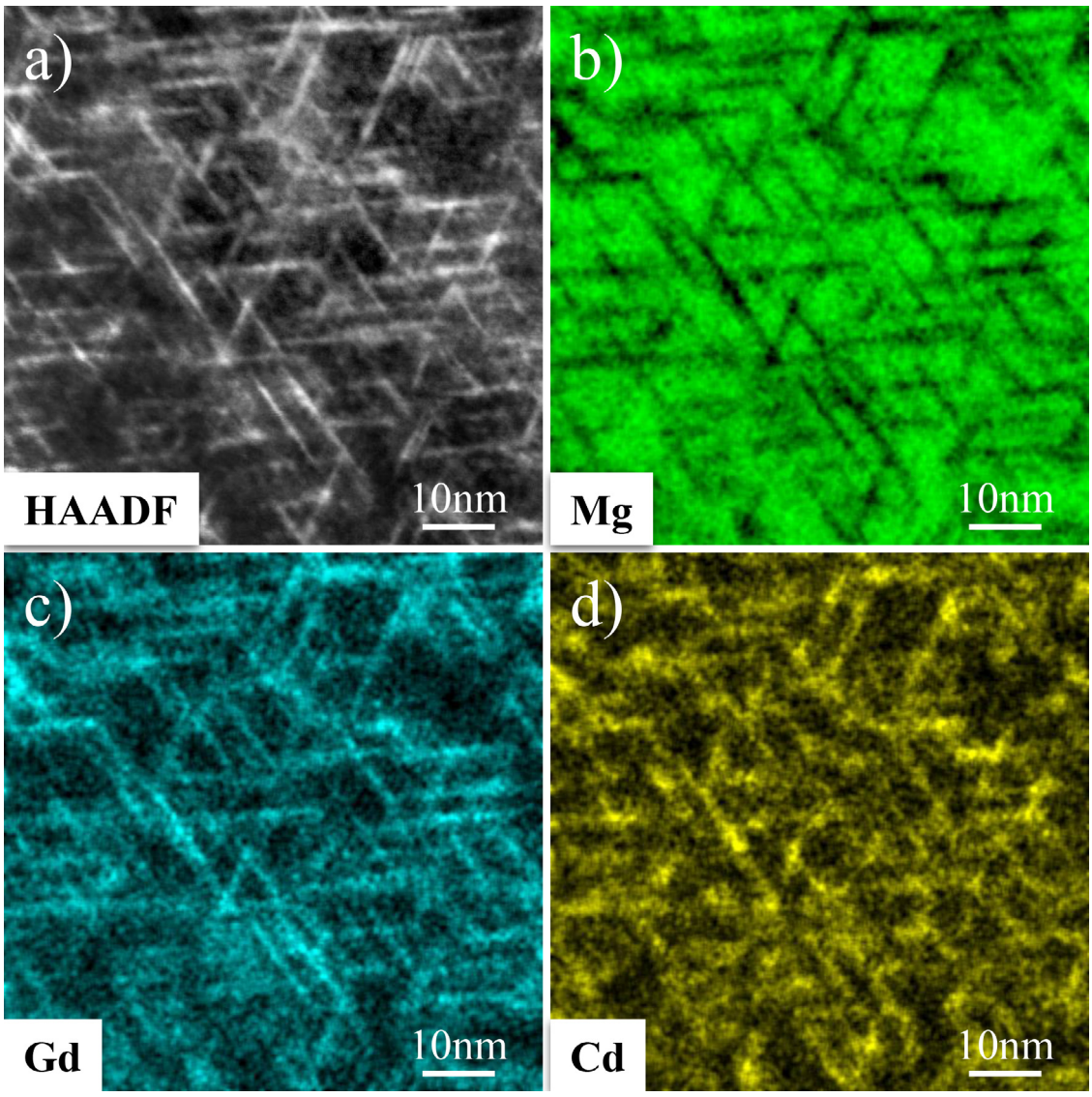

Fig. 6. EDS element mapping analysis for the long thin precipitates formed in the $Mg_{97}Gd_2Cd_1$ (at.%) alloy aged at 200 °C for 4 h. (a) HAADF-STEM image; (b) ~ (d) Element mapping images for Mg, Gd and Cd, respectively.

whole, most of these Gd-rich zigzag chain-like precipitates newly formed in this aging stage are still distributed with less correlation as compositional segregation products in the matrix, and herein they are referred to as G.P. II zones.

On the other hand, the matrix structure ordering was still underway. As can be seen in Fig. 5b, in addition to those B_{19}-type ordered domains (outlined with blue dashed lines), the other ordered domains of the $D0_{19}$-type were also formed coherently in the matrix together with B_{19}-domains. Fig. 5e is an atomic-scale HAADF-STEM image showing the structure of the $D0_{19}$-type ordered domain. Since the $D0_{19}$-type ordered domain is completely coherent with the Mg matrix by sharing the same symmetry of space group ($P6_3/mmc$), no any other additional orientational variant exist for it, and its diffraction pattern is similar to the pattern of Fig. 3b which is a result of multiple diffraction contribution from all the three types of orientational variants for B_{19}-domains (refer to Fig. 4). Actually, the coexistence of B_{19}- and $D0_{19}$-type domains is always in a coherently intergrowing state. For the sake of revealing the transition relationship between the two ordered structures, we will describe the $D0_{19}$-type structure using an orthogonal unit cell (see the lower unit cell depicted in Fig. 5e) instead of its usual rhombus one (see the upper unit cell in Fig. 5e). The detailed observation results concerning the B_{19}-to-$D0_{19}$ ordering transformation will be presented later in this section.

As early-stage Gd-rich precipitation products, G.P. I and G.P. II zones were observed to present in both B_{19}-type and $D0_{19}$-type domains (see Fig. 5f, in which the G.P. II zones tend to exhibit definite zigzag feature). The continuous evolution from (B_{19}-type domains + G.P. I zones) to ($D0_{19}$-type domains + G.P. II zones) in the early aging stage can bring about a complex mixture composed of the G.P. zones and ordered domains of different types (see Fig. 5b).

EDS analysis showed that both G.P. I and G.P. II zones are enriched with Gd and Cd. As can be seen in Fig. 6,

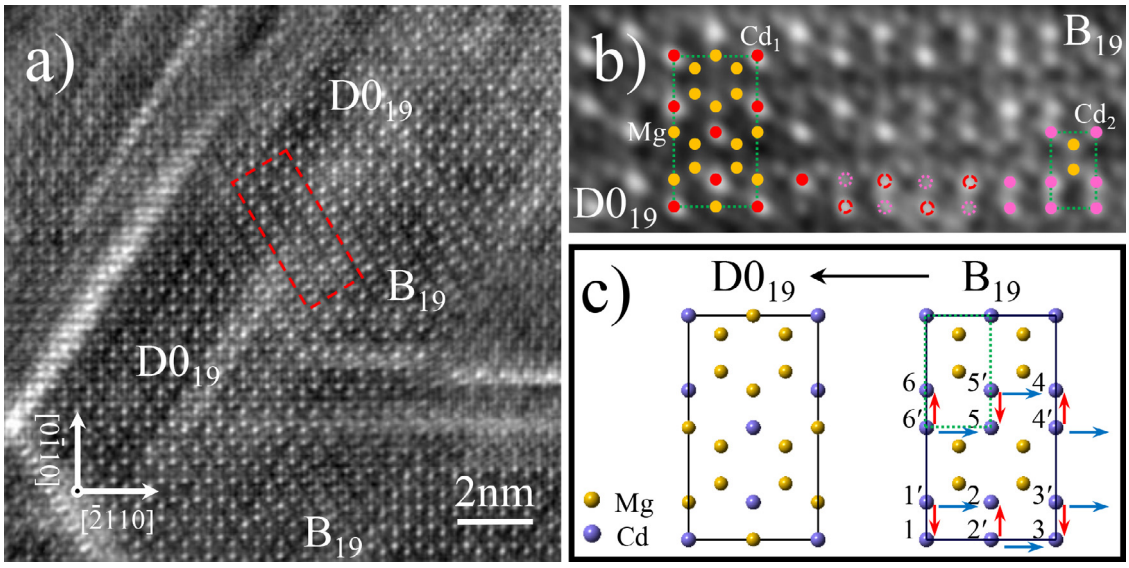

Fig. 7. (a) HAADF-STEM image recorded from the $Mg_{97}Gd_2Cd_1$ (at.%) alloy aged at 200 °C for 4 h, showing the intergrowth of B_{19} and $D0_{19}$ ordered structures; (b) Enlarged image of the region outlined with the red dashed rectangle presented in (a), showing the transition between B_{19} and $D0_{19}$ ordered structures; (c) Structural model showing the $B_{19} \rightarrow D0_{19}$ transformation.

where typical EDS mapping results for the G.P. zone precipitates formed at the early-aging stage (4 h) are presented, Gd-mapping image has quite sharp compositional contrast for exhibiting G.P. zone morphology in comparison with Cd-mapping one where the corresponding contrast is quite blurred. This indicates that the formation of G.P. zone precipitates (both G.P. I and G.P. II) is mainly dominated by the diffusion and precipitation of Gd atoms. The co-precipitation of Cd with Gd can enhance the G.P. zone precipitation, and this may then be favorable for the surrounding matrix structure ordering. It can be said that Gd and Cd are predominant for G.P. zone precipitation and ordered domain formation, respectively, even though minor mutual substitution between Gd and Cd atoms may occur during the formation of corresponding well-established structures.

The $D0_{19}$ and B_{19} domains can intergrow coherently, indicating that there exist close structural and compositional relationships between them. Fig. 7a is an atomic-scaled HAADF-STEM image showing a local ordered region being involved with the $B_{19} \rightarrow D0_{19}$ structural transition. As can be seen in Fig. 7b, which is the enlarged image of the region outlined with a red dashed rectangle in Fig. 7a, the Cd-rich atomic pillars in the $D0_{19}$ domain (Cd_1-pillars) exhibit brighter contrasts than that in the B_{19} domain (Cd_2-pillars), implying that the proportion of Cd atoms is higher in Cd_1-pillars than in Cd_2-pillars. In the $B_{19} \rightarrow D0_{19}$ transition region, the Cd_2-pillars in the B_{19} structure will adjust their Cd-content as reflected by the variation tendency of their Z-contrasts. For those Cd_2-pillars which coincide in position with the Cd_1-pillars in the $D0_{19}$ structure, their Z-contrasts turn to increasingly bright (such as the pillars marked with red dashed circles in Fig. 7b), whereas for the other Cd_2-pillars, their Z-contrasts will be weakened (such as those marked with pink dotted circles in Fig. 7b). These contrast variations strongly indicate that a re-distribution of Cd atoms can occur in the B_{19} structure through pillar-to-pillar diffusion so as to form Cd_1-pillars for constructing the $D0_{19}$ structure during the $B_{19} \rightarrow D0_{19}$ structural transformation. As illustrated in Fig. 7c, the extended $D0_{19}$-type Mg_3Cd unit cell (as we defined in Fig. 5e) can be established on the basis of a B_{19}-type MgCd supercell through the diffusing of Cd atoms from Cd_2-pillars $1' \sim 6'$ to Cd_2-pillars $1 \sim 6$. The Cd atoms in the pillar $1'$ could have two possible diffusion paths, $1' \rightarrow 1$ or $1' \rightarrow 2$, both of which are the nearest diffusion paths in an hcp-based structure. In order to clarify the actual diffusion path for the Cd atoms during the $B_{19} \rightarrow D0_{19}$ transformation, it is necessary to calculate the corresponding potential barrier through the first principle method so as to figure out the possible path with the lowest potential barrier for the Cd-atom diffusion. This effort will be made in our future work.

3.2.4. Formation of bamboo-raft-like β′ precipitates featured by stacking of long G.P. II zones

As the aging treatment at 200 °C continued to 18 h, the average length of G.P. zones had increased to ~30 nm (see Fig. 8a). In particular, bamboo-raft-like precipitates constructed by sequentially stacking three or more G.P. II zones in the $< 10\bar{1}0 >_{Mg}$ direction had been formed in many areas, such as those outlined with red ellipses in Fig. 8a. High-magnification HAADF-STEM observation clearly revealed that most of the structurally irregular G.P. I zones had transformed to well-defined G.P. II zones exhibiting characteristic zigzag-chain contrast, and that the on-growing G.P. II zones can be further combined into a bamboo-raft-like precipitation configuration featured by periodically stacking one after another in a mirror manner with an interval of ~1.11 nm (see Fig. 8b). Actually, the observed bamboo-raft-like precipitation structure built up by stacking well-defined G.P. II zones

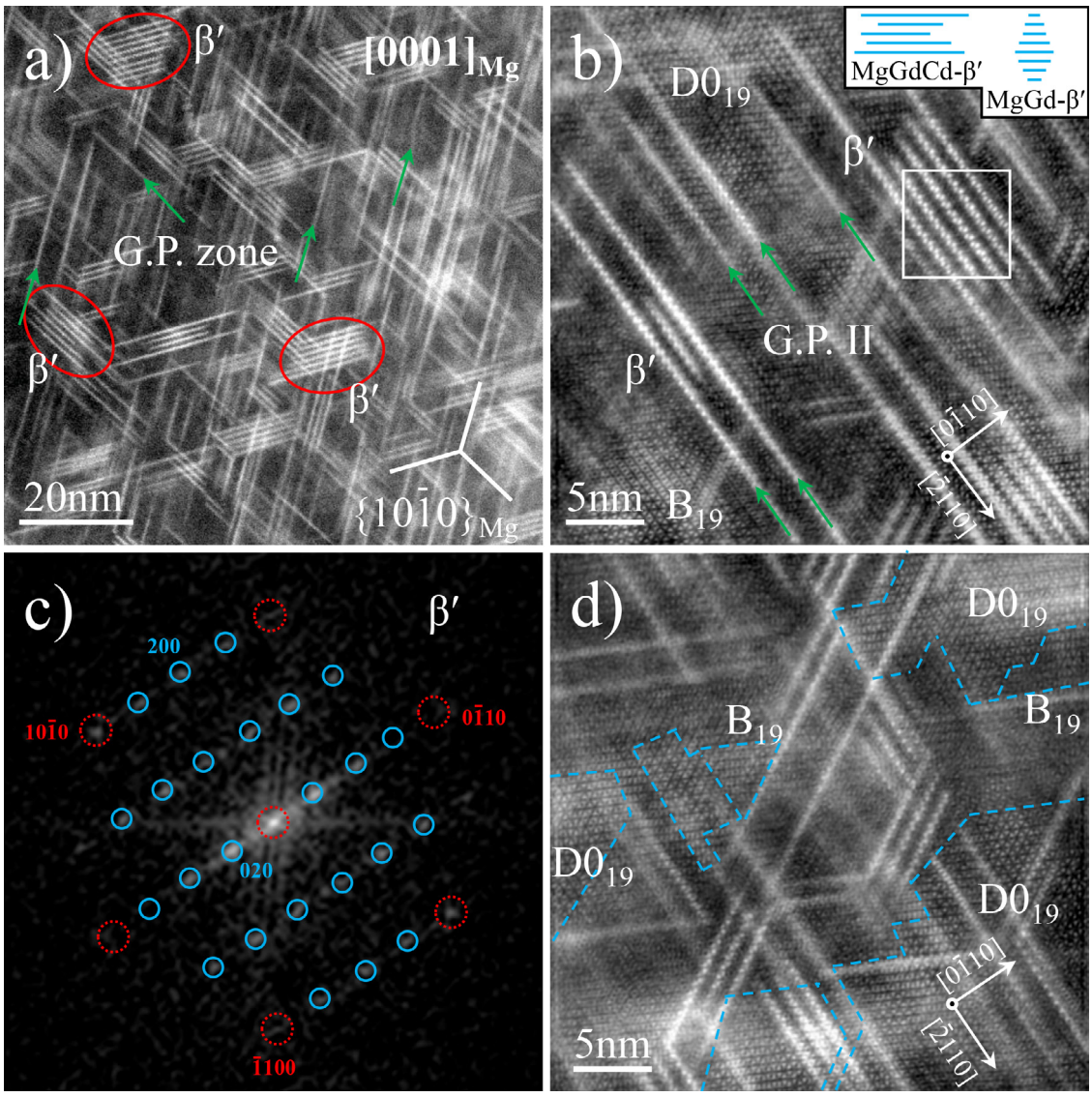

Fig. 8. (a) Low-magnification and (b, d) high-magnification HAADF-STEM images recorded from the $Mg_{97}Gd_2Cd_1$ (at.%) alloy aged at 200 °C for 18 h along its $[0001]_{Mg}$ axis; (c) FFT pattern corresponding to the region outlined with the white square in (b). For comparison, a schematic illustrating the morphological difference between Mg-Gd-Cd and Mg-Cd β' phases is inserted in (b).

is nothing but the β' phase structure, and this can be further confirmed from its corresponding FFT pattern (see Fig. 8c). Our observation offers a clear illustration showing that the nucleation and growth of the β' precipitate can be dominated by the formation and stacking of G.P. II zones, rather than by one-by-one formation and arrangement of individual β' unit cells. Obviously, it is the formation of G.P. II zones with a longer length in the ordered matrix that allows the β' phase constructed by stacking of them to have a bamboo-raft-like morphology. As illustrated in the inset in Fig. 8b, this characteristic morphology for the β' phases in our Mg-Gd-Cd alloy is obviously different from the common long-ellipsoidal morphology for those β' phases formed in Mg-Gd binary alloys.

Besides, close observation had shown that the matrix is still characterized by a mixture of B_{19}-type and $D0_{19}$-type domain structures (see Fig. 8d), which had no evident difference compared with the previous aging stage.

3.2.5. Precipitation and ordered structures corresponding to the peak aging

Further increasing the aging time to 25 h (corresponding to the peak-aging at 200 °C) brought about remarkable variation in precipitation structure. The typical HAADF-STEM observation results are presented in Fig. 9. It can be seen that, in addition to the densely distributed β' phases which had already been formed as main strengthening phase, a considerable number of newly formed precipitates with very bright Z-contrasts had also been formed to coexist with G.P. II zones and bamboo-raft-like β' phases (see Figs. 9(a∼c)). These precipitates with high Gd-content distribute mainly in between adjacent β' phases and have either granular or

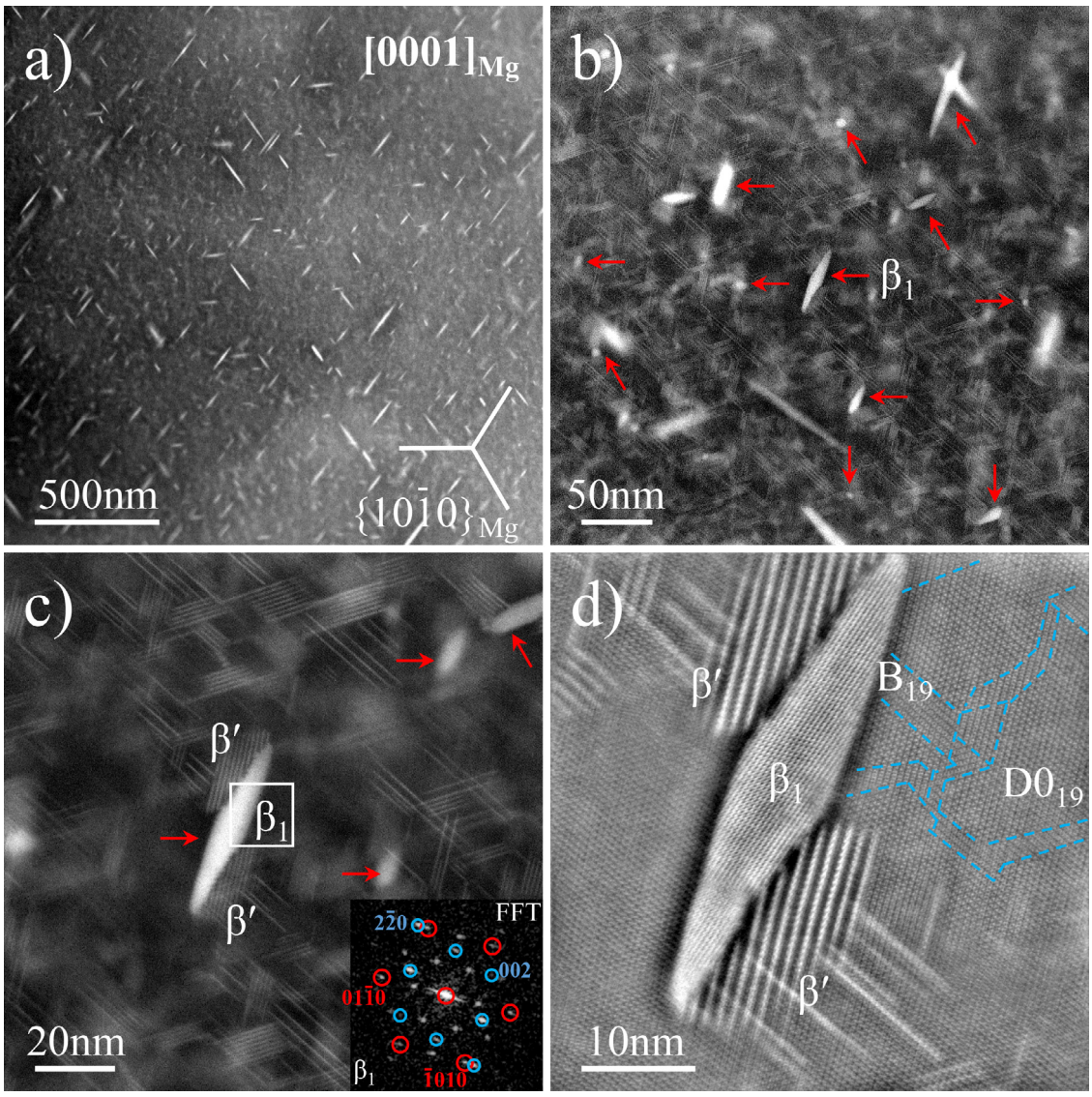

Fig. 9. HAADF-STEM observations of the precipitation structure along the $[0001]_{Mg}$ direction after the $Mg_{97}Gd_2Cd_1$ (at.%) alloy aged at 200 °C for 25 h. (a) Distribution of newly-formed Gd-rich precipitates (β_1 phases); (b) Formation of the β_1 phases coexisting with G.P.II zones and β' precipitates; (c) A typical β_1 phase growing with two attached β'-phases and its FFT pattern (inset) obtained from the region outlined with a white square; (d) FFT-filtered image showing the coexistence of various precipitates and ordered structure domains.

rhombic morphology (see those indicated by red arrows in Figs. 9(b, c)). Those granular precipitates are usually smaller than 10 nm in average diameter, while rhombic precipitates are relatively larger, with their average width and length being approximately 10 nm and 40 nm, respectively. As determined by atomic-scale HAADF imaging and the corresponding FFT pattern indexing (see Fig. 9d and the inset in Fig. 9c), the rhombic precipitate is structurally identical to the f.c.c.-structured β_1 phase which has been observed to be formed as non-equilibrium precipitate prior to the formation of equilibrium β phase in some Mg-RE based alloys [13,56-61]. The granular precipitates are actually some precursors of the β_1 phases, which can be regarded as β_1 embryos or nuclei with incomplete or imperfect β_1-structure. The detailed structural characterization for these β_1 precursors will be reported elsewhere. It should be pointed out that the solute Cd atoms can involve in the Gd-rich precipitation directly. The existence of Cd (6–7 at.%) in growing β_1 precipitates has been clearly revealed by means of EDS element mapping analysis (see Fig. 10). Notice also that the Cd-content in the well-developed β' structure is much lower than that in β_1 precipitates. Comparing the composition contrast for those β_1 phases coupled with β' phases in Figs. 10(a, c, d), where some typical β_1 and β' phases are indicated with red and yellow arrows, respectively, one can see that the Cd mapping contrast for these β' phases is much weaker (see Fig. 10d).

On the other hand, as seen in Fig. 9d, ordered domains of B_{19}- and $D0_{19}$-types still exist in the Mg matrix together with various Gd-rich precipitates. It can be said that establishing the coexistence of the dispersed G.P. II zones, $\beta' + \beta_1$ phases and ordered domains in the matrix is contributive to achieve adequate peak-hardness for the aged Mg-Gd-Cd

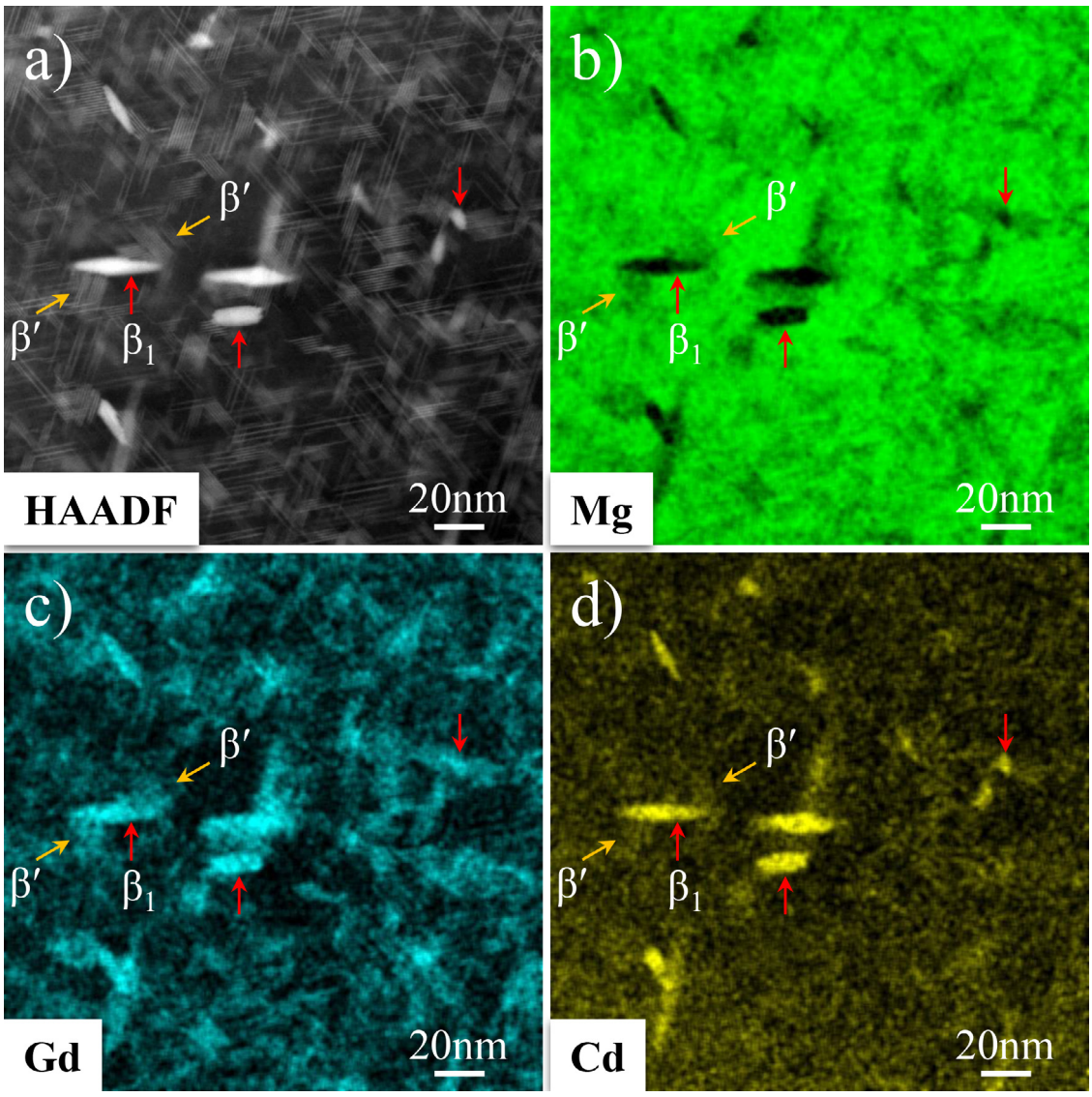

Fig. 10. EDS element mapping analysis for the growing precipitates in the $Mg_{97}Gd_2Cd_1$ (at.%) alloy aged at 200 °C for 25 h. (a) HAADF-STEM image in which some β_1 and β' phases are indicated with red and yellow arrows, respectively; (b) ~ (d) Corresponding element mapping images for Mg, Gd and Cd, respectively.

alloy. It appeared that the matrix ordering process had reached a relative equilibrium state at this peak aging stage since no pronounced evolution was observed for the ordered structures in comparison with the case of the near-peak aging in the previous stage.

3.2.6. Precipitation structure and evolution in the over-aging stage

After the Mg-Gd-Cd alloy getting through the peak aging, the solid-soluted content of Gd in the matrix will reduce drastically since massive Gd-rich precipitation has already taken placed before that. The formation of more β_1 phases followed by their coarsening would turn to be a major evolution process in the over-aging stage. With the aging time being extended to 36 h, the β_1 phases with high Gd-content exhibited obvious increases in both average dimension and number density (see Fig. 11a), whereas both the G.P. II zones and β' phases tended to be re-dissolved continuously. In fact, G.P. II zones had almost disappeared at this stage (see Fig. 11b). Nevertheless, the β'-β_1-β' coupled configuration, extensively existing at the peak-aging stage, can still remain in some region in addition to those fully grown β_1 phases (those large and isolated ones) (see Figs. 11b and 11c). It should be pointed out that Cd can directly involve in the formation of β_1 phases as a constituent element at this stage. This fact can be seen clearly in Fig. 12 where the EDS element mapping results for the β_1 precipitates formed at this stage are presented. The distribution of Cd is quite uniform in well-developed β_1 phases (see Fig. 12d), which is almost the same as that of Gd (see Fig. 12c).

As the aging time increased from 36 to 72 h, more β_1 phases with long-lath morphology were formed but their coarsening tendency appeared to be insignificant (see Fig. 11d and compare with Fig. 11a). The average size for

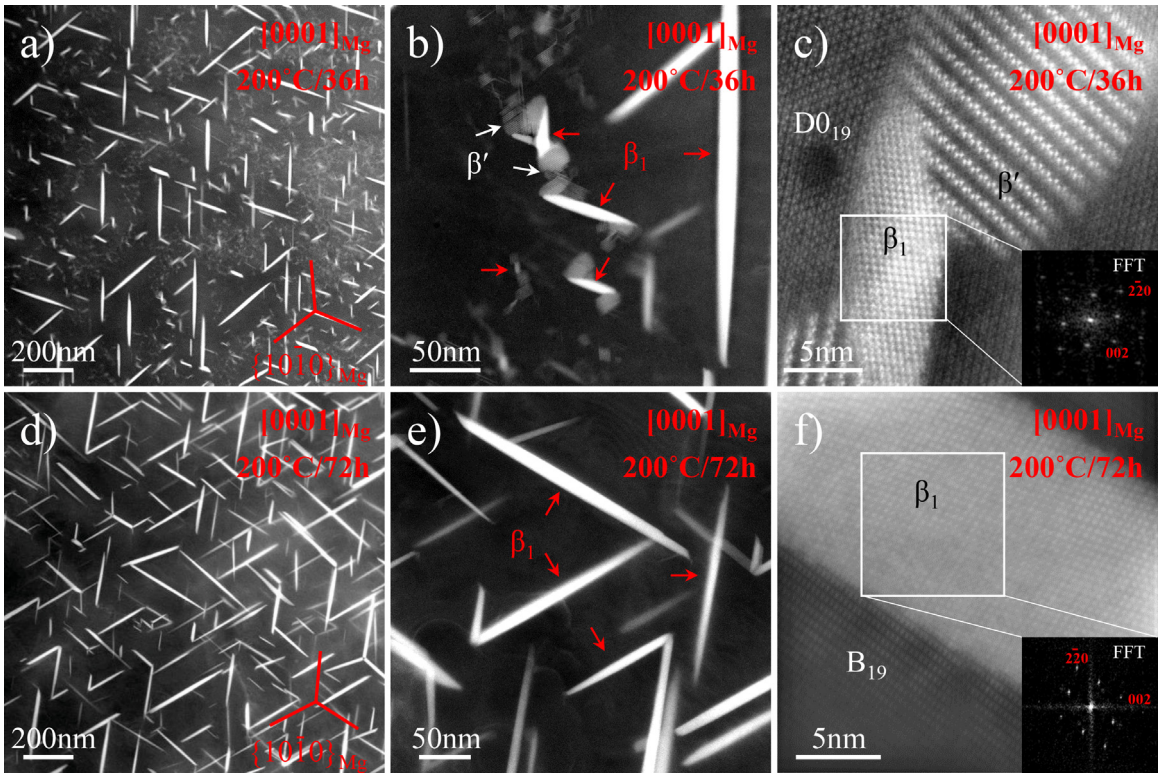

Fig. 11. HAADF-STEM images taken from the aged $Mg_{97}Gd_2Cd_1$ (at.%) alloy along the $[0001]_{Mg}$ axis, showing precipitation structures after aged at 200 °C for 36 h (a) ∼ (c) and 72 h (d) ∼ (f). The insets in (c) and (f) are the FFT patterns corresponding to the outlined regions.

the β_1 phases formed at this stage is estimated to be ∼15 nm in width and ∼350 nm in length, respectively (see Fig. 11d). In contrast, however, the β' phases attached to each end of the β_1 phases had virtually disappeared at this stage (see Fig. 11e). On the whole, the precipitation evolution at 200 °C had already entered a steady stage when the aging time was further extended to longer (> 72 h), and this corresponded well to the smooth tendency of the hardness variation for the aged Mg-Gd-Cd alloy, as seen from the corresponding hardening curve in Fig. 1.

On the other hand, it should be pointed out that the aging structural evolutions, including the coarsening of β_1 phases and the re-dissolving of β' phases in the over-aging stage, will bring about the continuous modification of the ordered structures in the matrix. Specifically, most β_1 phases formed after aging 36 h were observed to coexist with the $D0_{19}$ ordered structure (see Fig. 11c). However, a small number of local B_{19} ordered structure can still coexist with β_1 phases even though the Mg-Gd-Cd alloy had been aged for 72 h (see Fig. 11f). It should be pointed that the β_1 enriched with both Gd and Cd is a final equilibrium precipitation phase in the Mg-Gd-Cd alloy aged at 200 °C. With more and more Gd and Cd involving in the formation and coarsening of β_1 phases, the ordered structure domains around β_1 phases will tend to disappear finally due to the gradual lack of Cd in the matrix. We had confirmed that, when the aging further continued to 200 h, only equilibrium β_1 phases were formed without the coexistence of any surrounding ordered structure (see Fig. 13). It is obvious that Cd can play important roles in promoting the formation and stability of the β_1 phase. As for the β phase, which is well-known as an equilibrium phase in many aging-hardenable Mg-RE alloys, its formation was not found to occur in our Mg-Gd-Cd alloy during aging at 200 °C.

4. Discussion

4.1. Aging microstructure evolution in Mg-Gd-Cd alloy

From the above experimental observations, it has been made clear that the formation and evolution of Gd-rich precipitates in the Mg-Gd-Cd solid-solution alloy can take place in conjunction with the ordering transformation in the Gd/Cd-containing α-Mg matrix. Gd and Cd re-distributions are mainly responsible for the aging precipitation and the matrix structure ordering, respectively, although complex mutual influence may exist for Gd and Cd to involve in these processes. Four Gd-rich precipitates, G.P. I zone, G.P. II zone, β' and β_1, have been observed to be formed in the Mg-Gd-Cd alloy subjected to aging treatment at 200 °C. As a summary, the aging microstructure evolution involving the Gd-rich precipitation and the concurrent matrix structure ordering in the Mg-Gd-Cd alloy aged at 200 °C is schematically shown in Fig. 14. For clarity and convenience, let us first briefly describe the evolution scenario before discussing the effects of Cd-addition on aging hardening and Gd-rich precipitation behaviors in detail. As illustrated in Fig. 14, after the initial precipitation of the thin-plate G.P. I zones and the formation

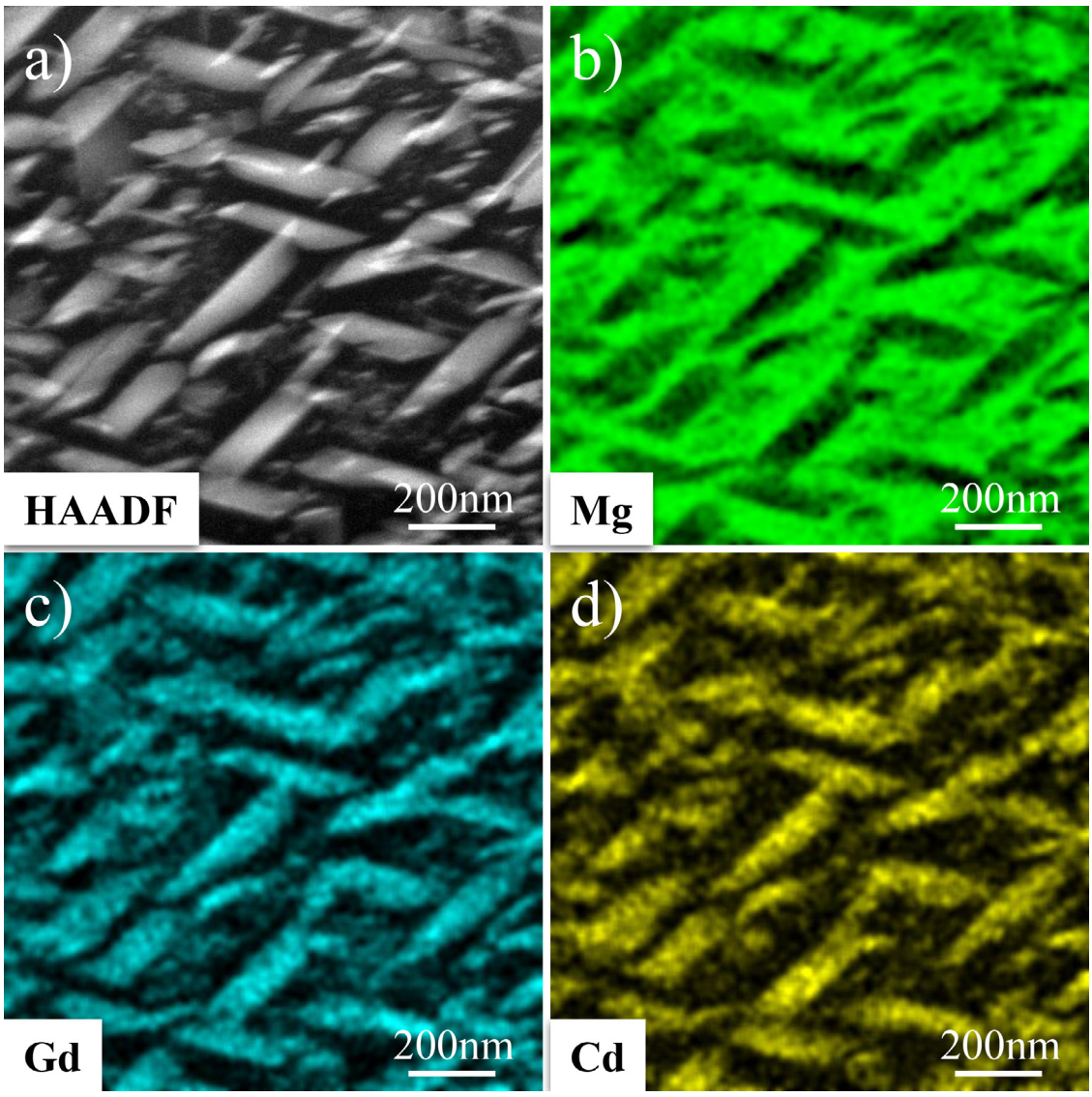

Fig. 12. EDS element mapping analysis for the β_1 precipitates formed in the $Mg_{97}Gd_2Cd_1$ (at.%) alloy aged at 200 °C for 36 h (the viewing direction is away from the $[0001]_{Mg}$ axis). (a) HAADF-STEM image; (b)∼(d) Element mapping images for Mg, Gd and Cd, respectively.

of B_{19}-type domains with three different orientational variants at the early aging stage (2 h), the aging structure soon evolved into a more complex mixture due to the further formation of G.P. II zones and $D0_{19}$-type domains (4 h). Subsequently, the β' phases initiated to be constructed basing on the characteristic stacking of G.P. II zones, during which the continuous $B_{19} \rightarrow D0_{19}$ ordering transformation in the domain matrix gradually led to a ($D0_{19} + B_{19}$) intergrowing state (4∼18 h). With more β' phases being formed as main precipitates, some f.c.c. β_1 phases with higher Gd-content began to nucleate in between the adjacent β' phases and finally grew to have a definite rhombic morphology (25 h, peak aging). These β_1 phases which actually have a three dimensions prismatic shape can steadily coarsen to form long thick lath precipitates with their surrounding G.P. II zones and β' phases being slowly re-dissolved (72 h). After the aging time is prolonged to 200 h, only equilibrium β_1 phases can finally be retained in the matrix (200 h). As a result, the aging-precipitation sequence for the Gd-rich phases in the Mg-Gd-Cd alloy can be described as: S.S.S.S. → G.P. I zone → G.P. II zone → β' phase → β_1 phase. Companying with this series of precipitation, the ordering transformation in the alloy matrix occurred in the following sequence: S.S.S.S. → B_{19} → $D0_{19}$. The concurrent occurrence of Gd-dominated precipitation and Cd-dominated ordering transformation can give rise to a more diverse aging microstructure in the aged Mg-Gd-Cd alloy.

Due to the coexistence of two aging evolution sequences in the Mg-Gd-Cd alloy during aged at 200 °C, the competition and influence between them are therefore inevitable with the aging progressing. At the very early stage of aging, the concurrent occurrence of Gd/Cd co-precipitation (G.P. I zone) and B_{19}-type structure ordering in the matrix can cause complex local aging structure during the re-distribution of Gd and Cd solutes (see Fig. 3). It should be pointed out that the ma-

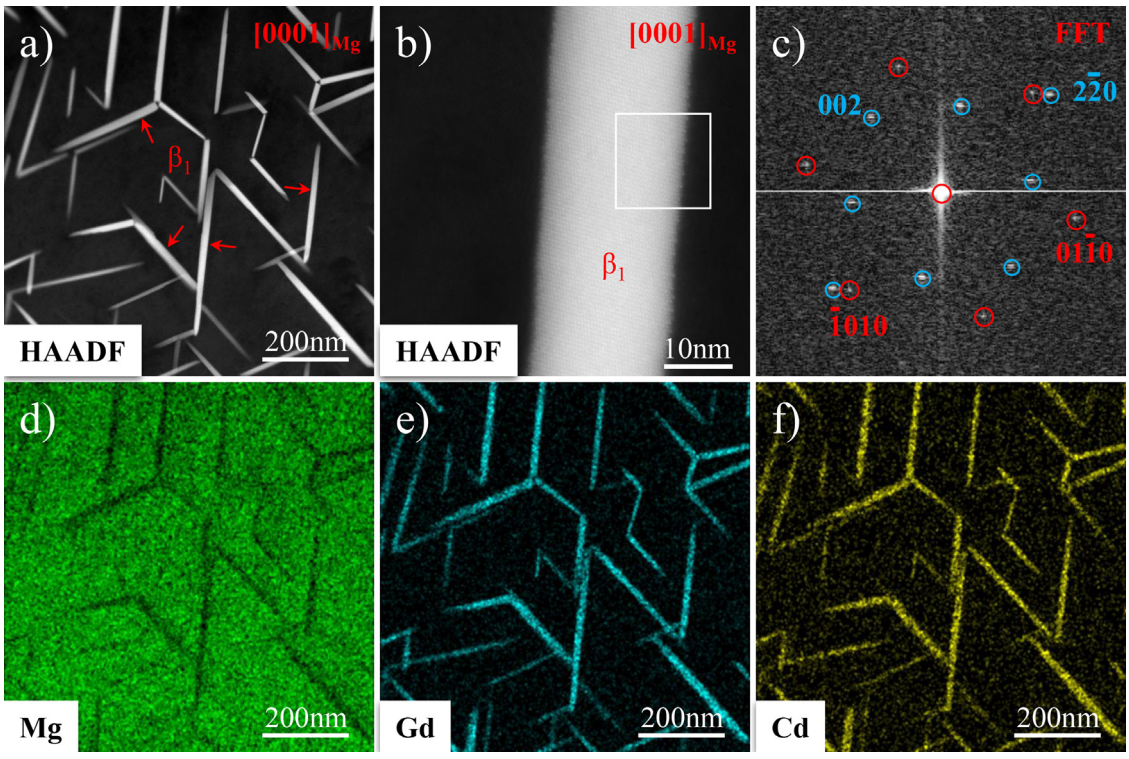

Fig. 13. Structural and compositional characterizations of the β_1 precipitates formed in the $Mg_{97}Gd_2Cd_1$ (at.%) aged at 200 °C for 200 h. (a) HAADF-STEM image showing the distribution of precipitated β_1 phases in the clean matrix; (b) Atomic-resolution HAADF-STEM observation showing that the β_1 phase was formed without surrounding ordered structure in the matrix; (c) FFT pattern corresponding to the outlined region in (b); (d)~(f) Element mapping images corresponding to (a) for Mg, Gd and Cd, respectively.

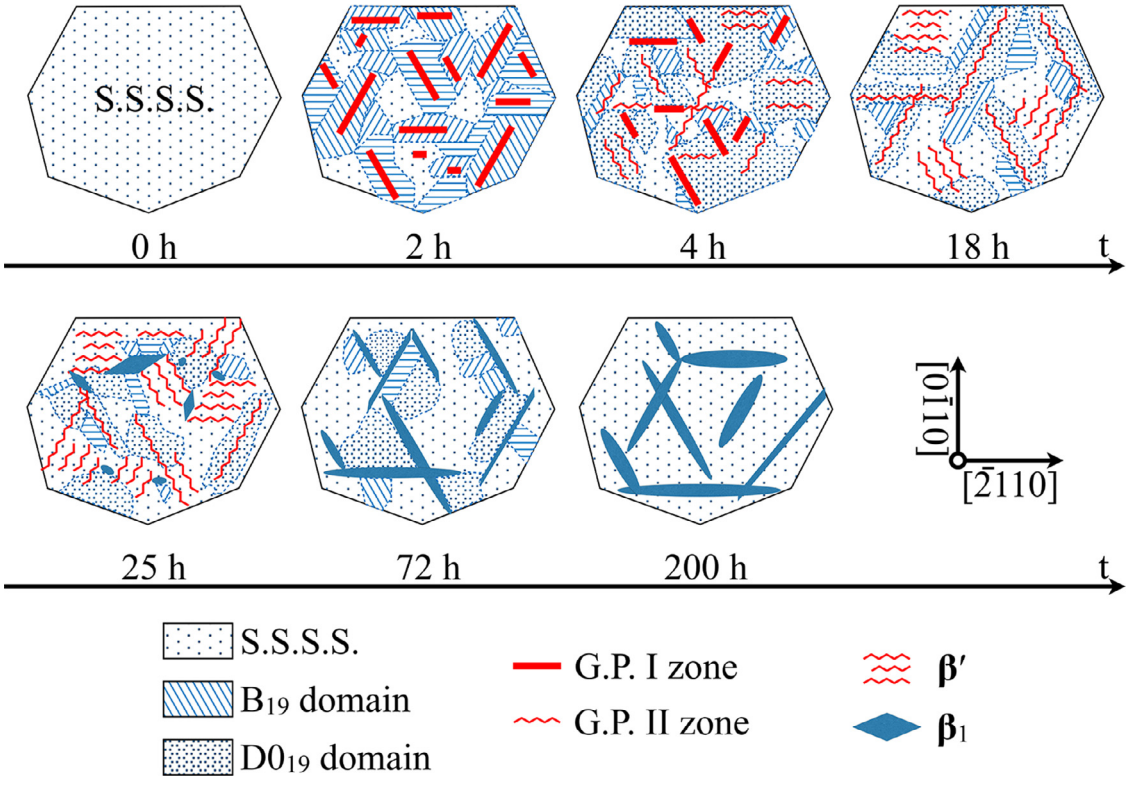

Fig. 14. Schematic diagram showing the ordering transformation and precipitation evolution in the Mg-Gd-Cd S.S.S.S alloy subjected to aging at 200 °C.

jority of G.P. I zones were observed to lie within the B_{19} domains or close to the domain boundaries (such as those indicated by red arrows in Fig. 3d or schematically illustrated in Fig. 14 (2 h)). However, this does not indicate that the G.P. I zones are formed relying on the B_{19} domains. It can be inferred that the segregation of G.P. I zones is ahead of the formation of well-definite B_{19}-type ordered domains, considering the fact that the G.P. I zones of Gd/Cd co-segregation have three equivalent habit planes which are consistent with three sets of $\{10\bar{1}0\}_{Mg}$ planes of the α-Mg matrix. It will be structurally and compositionally more favorable for Gd(Cd)-rich G.P. I zones to segregate from the Mg-Gd-Cd S.S.S.S. matrix directly. Otherwise, the G.P. I zone segregation will have to segregate along a high-index habit plane ($//\{10\bar{1}0\}_{Mg}$) in the Cd-enriched B_{19} ordered structure with low symmetry, and certainly, this is unlikely to occur. The matrix structure ordering dominated by Cd will be more prone to occur around the developing G.P. I zones since the relative Cd enrichment can occur there. This ordering process could disturb local Gd-rearrangement in the Mg matrix and thus lead to a less ordered arrangement of Gd atoms in the precipitated G.P. I zones. The long G.P. I zone is a new precipitation form that is absent in aged Mg-Gd binary alloys, but can be formed as the primary precipitation product coexisting with B_{19}-type ordered domains in our ternary Mg-Gd-Cd alloy aged at the early aging stage. Of course, the existence of solute Cd is a critical factor that can initially promote the formation of Gd(Cd)-rich G.P. I zone and then involve in the surrounding B_{19}-type ordering transformation so that the G.P. I zones can be enclosed in the ordered domains or in the vicinity of domain boundaries. A more detailed discussion concerning the effects of Cd on the Gd-rich precipitations at different aging stages will be given in Section 4.3.

In comparison with the evolution process of Gd-rich precipitation, that of ordered structures in the matrix appears to be inapparent since B_{19} and $D0_{19}$ ordered domains usually intergrow coherently, and their mixture can be observed at various aging stages (see Figs. 5,8,9,11). However, the $B_{19} \rightarrow D0_{19}$ ordering transformation, exhibiting a continuous transitional mechanism as we have presented in Section 3.2.3 (see Fig. 7), is actually affected by the modifications of local solute composition and diffusion condition around Gd-rich precipitation phases. With the Gd-rich precipitation progressing in sequence, the surrounding ordered structures will have to undergo some changes to achieve a relative equilibrium correspondingly. In the pre-peak aging stage, with the continuous S.S.S.S. $\rightarrow B_{19} \rightarrow D0_{19}$ ordering transformation and the increasing of number density for the β' phases, the networking of differently-orientated β' phases and G.P. zones may close off some local regions where the long-range Cd diffusion may be hampered so that localized equilibrium for the ordering transformation can be established provisionally. As clearly revealed by the EDS analysis, Cd can directly involve in the precipitation of β_1 phases (see Fig. 10). Specially in the over-aging stage, a large amount of Cd will be consumed to involve in the formation and coarsening of Gd/Cd-rich β_1 phases (see Fig. 12). The variations in the precipitation density and configuration of Gd/Cd-rich β_1 phases will alter the surrounding Gd- and Cd-concentrations, and owing to this, the relative equilibrium state for the ordered structure domains in the matrix will have to be re-established. Therefore it is not unexpected that either B_{19} or $D0_{19}$ ordered structure could be retained or dissolved or even re-formed locally in the surrounding of some β_1 phases even though the sample has already been subjected to over-aging for a long time (see Fig. 11). It should be pointed out that the β_1 phase is the only equilibrium phase in the $Mg_{97}Gd_2Cd_1$ (at.%) alloy aged at 200 °C. The ordered structure of either B_{19}- or $D0_{19}$-type around β_1 phases will finally disappear completely if the over-aging time is sufficiently long (for instance, 200 h) (see Fig. 13).

4.2. Relation between aging hardening behavior and microstructure

Through the mutual contrast between the isothermal aging hardening behavior reflected by the aging hardness curve of the $Mg_{97}Gd_2Cd_1$ alloy presented in Fig. 1 and the aging microstructure evolution illustrated in Fig. 14, one can easily figure out the interrelation between them. The under-aging process (t = 0–25 h) for the Mg-Gd-Cd alloy can be roughly divided into three stages according to the characteristic variations in both aging hardening feature and microstructure before the hardness increases to the peak value (~110 HV).

In stage I (t = 0–2 h), the hardening rate is mainly dominated by the G.P. I zone segregation. For the Mg-Gd-Cd S.S.S.S. alloy sample with an initial hardness value of ~72 HV, aging at 200°C for 2 h allows its hardness value to increase to ~97 HV (approximate 88% of the peak value). This rapid increase of hardness can be attributed to the quick segregation of densely distributed long G.P. I zones along with the B_{19} ordering in the surrounding matrix. For the aged $Mg_{98}Gd_2$ sample, however, both its hardness value and hardening rate are lower in the same stage (see the green hardening curve in Fig. 1), and no G.P. I zone can be formed except for some very short zigzag chains of G.P. II zones and prosperous nano-sized atom clusters of Gd atoms (see the inset in Fig. 3c). Obviously, it is due to the extraordinary effect on precipitation features arising from the Cd-addition that allows the Mg-Gd-Cd alloy to have a much swift hardening response in its early aging stage.

In stage II (t = 2–4 h), hardness variation exhibits a plateau, as seen in Fig. 1, indicating that the hardening rate begins to slow down when aging to this stage. Actually, the aging microstructural evolutions corresponding to the plateau have been clearly revealed to involve the following structural transformation: (G.P. I zones + B_{19} ordered domains) (2 h) $\rightarrow$ (G.P. II zones + $D0_{19}$ ordered domains) (4 h) (see Fig. 14). It seems that the $D0_{19}$- and B_{19}-ordered domains can play the same role in strengthening the alloy matrix since the obvious $B_{19} \rightarrow D0_{19}$ ordering transformation occurring in this stage exhibits less effect on the further increment of hardness. However, in contrast to the G.P. I zone with a less definite structure, the G.P. II zone with an ordered zigzag Gd(Cd)

array should act as a more effective strengthening precipitate. Nevertheless, the G.P. I → G.P. II structural transformation will contribute effectively to the hardness increment only when the formation of G.P. II zones has reached a sufficient number density. This is also a necessary condition for the subsequent β' formation.

In stage III (t = 4–25 h (peak aging)), the hardening rate is accelerated again due mainly to the precipitation of the β' phases. With increasing the number densities of G.P. II and β' precipitates during which the β_1 precipitation is also initiated, the aging hardness will keep increasing until a peak value is achieved after aging for 25 h. The peak aging microstructure for the Mg-Gd-Cd alloy is characterized by a complex mixture involving G.P. II zones, β' phases, β_1 phases, B_{19}- and $D0_{19}$-type domains, in which the contribution of β' precipitates to the aging hardness increment is dominant. Of course, more extensive formation of various ordered domains in the Mg matrix will have benefits for enhancing alloy strength in that they can hinder the dislocation motion more effectively during deformation.

As for the hardening behavior of the Mg-Gd-Cd alloy in the over-aging stage (t > 25 h), the hardness decrease is mainly due to the facts that the densely-distributed β' precipitates are re-dissolved gradually and the formation of Gd/Cd-rich β_1 phases has become a predominant process. In contrast, the hardness of aged Mg-Gd alloy can be sustained at a high level in the aging stage of t = 50–200 h (see the green curve in Fig. 1), since the formation of the Mg-Gd β_1 phase through dissolving surrounding β' precipitates has rarely been observed to occur in Mg-Gd alloys aged at 200 °C. The equilibrium Mg-Gd-Cd β_1 phases with definite long-lath morphology and uniform distribution configuration can be formed at 200 °C when the aging time is sufficiently long (72–200 h), and due to this, the aging hardness for the Mg-Gd-Cd alloy fully aged at 200 °C can be maintained at ~92 HV. In view of diverse aging microstructural evolution processes in the Mg-Gd-Cd alloy as we have presented above, it seems that the mechanical performance could be regulated more flexibly and efficiently for the Mg-Gd-Cd alloy than for a Mg-Gd alloy.

4.3. Effects of Cd on the Gd-rich precipitation

Adding Cd as an alloying element can be regarded as an effective controlling factor for the Gd-rich precipitation in that the Mg-Gd-Cd alloy indeed has shown apparent differences in precipitation dynamics, precipitate distribution and morphology in comparison with the $Mg_{98}Gd_2$ alloy and those previously reported Mg-Gd binary alloys. Specifically, we will discuss the effects of Cd on the Gd-rich precipitation in the following aspects.

(1) Effect on the Gd-rich G.P. zone precipitation at early aging stage

In comparison with the aged $Mg_{98}Gd_2$ alloy and those previously-reported Mg-Gd alloys [13,14] in which only hexagonal solute clusters and very short zigzag chains of Gd-rich G.P. II zones can be precipitated prior to the β' phase formation, the aged Mg-Gd-Cd alloy allows to precipitate quite long Gd(Cd)-rich G.P. I zones at the very early stage of aging. It should be pointed out that, for the ordered hexagonal Gd clusters which are prosperous in Mg-Gd alloys as a kind of common early-stage precipitation product, its formation is suppressed in the aged Mg-Gd-Cd alloy. Instead, quick Gd-segregation involving 2–4 atomic layers can occur along the three equivalent $\{10\bar{1}0\}_{Mg}$ planes, resulting in the formation of G.P. I zones with a long length (see Figs. 3(d–f)). This early-stage precipitation process is responsible for the swift hardening response in stage I, as we have mentioned above. It appears that the Gd atom diffusion in the Mg-Gd-Cd alloy is promoted in the Cd-solid-soluted matrix. As clearly revealed by our EDS analysis, Cd can co-segregate with Gd at the early aging stage, and this will help the Gd-dominant G.P. I zones to precipitate quickly with a long length but a less definite structure.

The Gd(Cd)-rich G.P. I zones existing with a less definite structure in B_{19}-type domains are not structurally stable, and they are prone to transform into more ordered G.P. II zones with the progressing of aging. Furthermore, a continuous ordering transformation from the B_{19} domain variants to the $D0_{19}$-type domains with a higher structural symmetry will be conducive to the formation of much longer zigzag chains of G.P. II zones along three equivalent $\{10\bar{1}0\}_{Mg}$ planes. Certainly, unlike the case in aged Mg-Gd alloys, the precipitation of unusually long G.P. I and G.P. II zones, together with the ordering transformation in the Mg-Gd-Cd alloy matrix at the early aging stage, will affect the subsequent Gd-rich precipitation evolution significantly.

(2) Effect on the formation of β' and related transitional precipitates

For the β' phase, which is widely known as a kind of main strengthening phase in many age-hardenable Mg-RE based alloys [13,48-54], its structure can be described as a periodic stacking of G.P. II zones (zigzag-featured layers) at regular intervals of α-Mg layers. In Mg-Gd binary alloys, the precipitated Mg-Gd β' phases are all characterized by the stacking of G.P. II zones with a very short length (see the inset in Fig. 8b), and therefore they usually exhibit a long ellipsoidal morphology [13,14]. In addition, the existence of various transition precipitates around individual β' phases or in between two adjacent β' phases had also been found in Mg-Gd alloys. Some typical Mg-Gd transition precipitates include: the β'_t phase constructed only by stacking short zigzag Gd-rich G.P. II zones but having a shorter stacking period [14,48,54], the β_M phase composed of only hexagonal Gd-rich atom clusters [13], and irregular hybrid precipitate consisted of both hexagonal and zigzag arrays of Gd-rich atom pillars [13,48,54]. Moreover, these transition precipitates can connect β' phases alternately to form long linear precipitation configurations [54]. However, through adding Cd as alloying element, all of these characteristics associated with the β' phase in the Mg-Gd alloy system can be altered significantly. Unlike the Mg-Gd β' phases in Mg-Gd binary alloys, the Cd-contained Gd-rich β' phases formed in our aged Mg-Gd-Cd ternary alloy can have an unusual bamboo-raft-like morphol-

ogy (see Figs. 8(a, b)). This is no unexpected considering that the G.P. II zones can be formed with a length much longer in the Mg-Gd-Cd alloy than in Mg-Gd alloys. Also, none of the above-mentioned Mg-Gd transitional precipitates was found to be formed in the aged Mg-Gd-Cd alloy. It has been reported that the formation of β' phase in an aged Mg-Gd alloy could cause considerable local strains due to the volume expansion of β' phase with respect to the alloy matrix [51]. The localized Gd-rich transitional precipitation could therefore be a result of local strain-accommodation. As we have clearly revealed, the formation of β' phases in the Mg-Gd-Cd alloy is accomplished by the stacking of the G.P. II zones which can grow longer in length in the ordered domains. The bamboo-raft-like Mg-Gd-Cd β' phase formed in this way can have a relatively low interfacial energy which will introduce less or no strain in its surrounding ordered matrix. Therefore, the strain-induced transitional precipitation associated with the β' phase will not occur in the Mg-Gd-Cd alloy.

(3) Effect on the β_1 phase formation

The β_1 precipitate phase in the Mg-Gd-Cd alloy can be formed extensively as an equilibrium phase during the aging at 200 °C. In contrast, for the β_1 phase in Mg-Gd alloys, its formation generally requires a higher aging temperature (> 250 °C) and longer aging time (> 500 h) [13,60], and furthermore, its number density is also much lower than that in the Mg-Gd-Cd alloy. Very recently, it has been shown through HAADF-STEM observation that the β_1 phases in Mg-Gd alloys are formed relying closely on the preexisting transitional precipitates [13]. However, our HAADF-STEM observations can clearly reveal that the formation of β_1 phase in the aged Mg-Gd-Cd alloy is independent of any of the above-mentioned transitional precipitate since no similar one can be formed to coexist with β' phases prior to the β_1 formation. As an alloying element with infinite solid solution ability in Mg, Cd can also involve in the Gd-rich β_1 precipitation directly in addition to its contribution to the matrix structure ordering. Cd element can be regarded as a β_1 stabilizer. Its uniform distribution in the well-grown β_1 phases in the Mg-Gd-Cd alloy has been clearly revealed by the EDS mapping analysis (see Figs. 10,12,13). Since the β_1 phases can precipitate more densely and have a number density much higher in the aged Mg-Gd-Cd alloy than in aged Mg-Gd alloys, it can be said that the adding of Cd is favorable for promoting the formation ability and stability of the β_1 phase. These effects of the Cd-addition on the β_1 formation are supposed to be beneficial for enhancing the high-temperature structural stability of Mg-Gd-based alloys.

On the whole, from our careful HAADF-STEM observation results and above discussions, it is clear that the effect of Cd alloying addition on the Gd-precipitation-dominated aging microstructure evolution in a Mg-Gd alloy can be multifold, including the introduction of structure ordering of different types for the matrix and the modifications in formation, morphology, distribution and evolution for the Gd-rich precipitates. Solute atom Cd can involve in the Gd-rich precipitation process directly. The addition of a proper amount of Cd can modify Gd-precipitation dynamics and thus can be taken as an effective precipitation controlling factor for the age-hardenable Mg-Gd-based alloy system.

5. Conclusions

In the present study, the aging microstructural evolutions in the $Mg_{97}Gd_2Cd_1$ (at.%) alloy subjected to the aging treatment at 200 °C, involving the ordering transformation in the alloy matrix and concurrent formation of the Gd-rich precipitates, have been characterized via HAADF-STEM imaging technique. The main conclusions are summarized as follows:

(1) The B_{19}-type ordered domains with three symmetrical orientation variants were formed together with Gd(Cd)-rich G.P. I zones from the Mg-Gd-Cd random S.S.S.S. matrix at the early aging stage, and then they gradually transformed to the $D0_{19}$-type ordered domains during the subsequent aging stage. The atomic ordering transformation process in the matrix is revealed to be: S.S.S.S. $\rightarrow$ B_{19}-type domains $\rightarrow$ $D0_{19}$-type domains. The continuous B_{19}-to-$D0_{19}$ structural transformation had been observed, which was mainly dominated by Cd atom diffusion and was accomplished through the re-arrangement of Cd atom pillars.

(2) Four Gd-rich precipitates, G.P. I zones, G.P. II zones, β' and β_1 phases, were observed to be formed in the Mg-Gd-Cd alloy during the aging at 200 °C, companying with the continuous matrix structure ordering. The G.P. I zone, which is a Gd/Cd co-precipitation product absent in the Mg-Gd system, is characterized as a long Gd(Cd)-rich segregation platelet along a $\{10\bar{1}0\}_{Mg}$ habit plane with 2 $\sim$ 4 atomic layers in thickness. The Gd-rich precipitation sequence in the aged Mg-Gd-Cd alloy is as follows: S.S.S.S. $\rightarrow$ G.P. I zone $\rightarrow$ G.P. II zone $\rightarrow$ β' phase $\rightarrow$ β_1 phase. Solute Cd atoms can involve in the formation of Gd-rich β' and β_1 phases in different extent. The Cd-distribution in the β' phases formed during aging from under-aging to peak-aging stages is relatively less and nonuniform, while that in the well-grown β_1 phases formed mainly in the over-aging stage is more obvious and quite homogeneous.

(3) Under the influence of Cd solutes and the related matrix structure ordering, the aged Mg-Gd-Cd alloy exhibited noticeable differences in the early-stage G.P. zone structure, morphology of β' precipitates and formability of β_1 phase in comparison with Mg-Gd alloys. The Gd precipitation in the under-aging stage can be effectively promoted. In particular, the Gd/Cd co-precipitation in the form of G.P. I zone and concurrent occurrence of matrix structure ordering are responsible for the swift aging hardening response in the early aging stage. Element Cd can act as a stabilizer for the β_1 phase, and its addition can allow a uniform distribution of equilibrium Mg-Gd-Cd β_1 phases to be established in the over-aging stage at 200 °C.

Declaration of competing interest

The authors declare that they have no known competing financial interests or personal relationships that could have appeared to influence the work reported in this paper.

Acknowledgment

The authors would like to acknowledge the financial supports from the National Natural Science Foundation of China [grant number 11274027] and Beijing Municipal Natural Science Foundation [grant number 2092005].

References

[1] L.L. Rokhlin, Magnesium Alloys Containing Rare Earth metals: Structure and Properties, Taylor & Francis, London; New York, 2003.
[2] J.F. Nie, Precipitation and hardening in magnesium alloys, Metall. Mater. Trans. A 43a (2012) 3891–3939.
[3] I. Polmear, D. StJohn, J.F. Nie, M. Qian, Light Alloys: Metallurgy of the Light Metals, Butterworth-Heinemann, Boston, 2017.
[4] B.L. Mordike, T. Ebert, Magnesium - properties - applications - potential, Mat. Sci. Eng. A-Struct. 302 (2001) 37–45.
[5] A.A. Luo, Recent magnesium alloy development for elevated temperature applications, Int. Mater. Rev. 49 (2004) 13–30.
[6] V. Neubert, I. Stulikova, B. Smola, A. Bakkar, B.L. Mordike, Corrosion behaviour of highly creep resistant magnesium-rare-earth-based alloys, Kovove Mater 42 (2004) 31–41.
[7] S. Tekumalla, S. Seetharaman, A. Almajid, M. Gupta, Mechanical properties of magnesium-rare earth alloy systems: a review, Metals (Basel) 5 (2015) 1–39.
[8] K. Gusieva, C.H.J. Davies, J.R. Scully, N. Birbilis, Corrosion of magnesium alloys: the role of alloying, Int. Mater. Rev. 60 (2015) 169–194.
[9] N. Mo, Q.Y. Tan, M. Bermingham, Y.D. Huang, H. Dieringa, N. Hort, M.X. Zhang, Current development of creep-resistant magnesium cast alloys: a review, Mater. Des. 155 (2018) 422–442.
[10] B.L. Mordike, Creep-resistant magnesium alloys, Mat. Sci. Eng. A-Struct. 324 (2002) 103–112.
[11] M. Nishijima, K. Yubuta, K. Hiraga, Characterization of β' precipitate phase in Mg-2 at% Y alloy aged to peak hardness condition by high-angle annular detector dark-field scanning transmission electron microscopy (HAADF-STEM), Mater. Trans. 48 (2007) 84–87.
[12] E.L.S. Solomon, A.R. Natarajan, A.M. Roy, V. Sundararaghavan, A. Van der Ven, E.A. Marquis, Stability and strain-driven evolution of β' precipitate in Mg-Y alloys, Acta Mater 166 (2019) 148–157.
[13] Y. Zhang, W. Rong, Y.J. Wu, L.M. Peng, J.F. Nie, N. Birbilis, A detailed HAADF-STEM study of precipitate evolution in Mg-Gd alloy, J. Alloy. Compd. 777 (2019) 531–543.
[14] M. Nishijima, K. Hiraga, Structural changes of precipitates in an Mg-5 at% Gd alloy studied by transmission electron microscopy, Mater. Trans. 48 (2007) 10–15.
[15] J.F. Nie, B.C. Muddle, Characterisation of strengthening precipitate phases in a Mg-Y-Nd alloy, Acta Mater 48 (2000) 1691–1703.
[16] D.Q. Li, Q.D. Wang, W.J. Ding, Precipitate phases in the Mg-4Y-4Sm-0.5Zr alloy, J. Alloy. Compd. 465 (2008) 119–126.
[17] K.Y. Zheng, J. Dong, X.Q. Zeng, W.J. Ding, Precipitation and its effect on the mechanical properties of a cast Mg-Gd-Nd-Zr alloy, Mat. Sci. Eng. A-Struct. 489 (2008) 44–54.
[18] N.Y. Liu, Z.Y. Zhang, L.M. Peng, W.J. Ding, Microstructure evolution and mechanical properties of Mg-Gd-Sm-Zr alloys, Mat. Sci. Eng. A-Struct. 627 (2015) 223–229.
[19] X. Gao, J.F. Nie, Enhanced precipitation-hardening in Mg-Gd alloys containing Ag and Zn, Scr. Mater. 58 (2008) 619–622.
[20] J.F. Nie, K. Oh-ishi, X. Gao, K. Hono, Solute segregation and precipitation in a creep-resistant Mg-Gd-Zn alloy, Acta Mater 56 (2008) 6061–6076.
[21] Y.M. Zhu, A.J. Morton, J.F. Nie, The 18R and 14H long-period stacking ordered structures in Mg-Y-Zn alloys, Acta Mater 58 (2010) 2936–2947.
[22] K. Saito, A. Yasuhara, K. Hiraga, Microstructural changes of Guinier-Preston zones in an Mg-1.5 at% Gd-1 at% Zn alloy studied by HAADF-STEM technique, J. Alloy. Compd. 509 (2011) 2031–2038.
[23] K. Kishida, H. Yokobayashi, H. Inui, M. Yamasaki, Y. Kawamura, The crystal structure of the LPSO phase of the 14H-type in the Mg-Al-Gd alloy system, Intermetallics 31 (2012) 55–64.
[24] Q.Q. Jin, C.F. Fang, S.B. Mi, Formation of long-period stacking ordered structures in $Mg_{88}M_5Y_7$ (M = Ti, Ni and Pb) casting alloys, J. Alloy. Compd. 568 (2013) 21–25.
[25] Q.Q. Jin, X.H. Shao, X.B. Hu, Z.Z. Peng, X.L. Ma, New polytypes of LPSO structures in an Mg-Co-Y alloy, Philos. Mag. 97 (2017) 1–16.
[26] C. Liu, Y.M. Zhu, Q. Luo, B. Liu, Q.F. Gu, Q. Li, A 12R long-period stacking-ordered structure in a Mg-Ni-Y alloy, J. Mater. Sci. Technol. 34 (2018) 2235–2239.
[27] Y. Zhang, Y.M. Zhu, W. Rong, Y.J. Wu, L.M. Peng, J.F. Nie, N. Birbilis, On the Precipitation in an Ag-Containing Mg-Gd-Zr Alloy, Metall. Mater. Trans. A 49a (2018) 673–694.
[28] H. Zhang, C.Q. Liu, Y.M. Zhu, H.W. Chen, L. Bourgeois, J.F. Nie, Revisiting building block ordering of long-period stacking ordered structures in Mg–Y–Al alloys, Acta Mater 152 (2018) 96–106.
[29] X.F. Gu, T. Furuhara, T. Kiguchi, T.J. Konno, L. Chen, P. Yang, On the atomic structure of γ'' phase in Mg-Zn-Gd alloy, Scr. Mater. 146 (2018) 64–67.
[30] X.F. Gu, T. Furuhara, L. Chen, P. Yang, Study on the planar segregation of solute atoms in Mg-Al-Gd alloy, Scr. Mater. 150 (2018) 45–49.
[31] Y. Kawamura, T. Kasahara, S. Izumi, M. Yamasaki, Elevated temperature $Mg_{97}Y_2Cu_1$ alloy with long period ordered structure, Scr. Mater. 55 (2006) 453–456.
[32] Z.R. Liu, D.Y. Li, The electronic origin of strengthening and ductilizing magnesium by solid solutes, Acta Mater 89 (2015) 225–233.
[33] A. Issa, J.E. Saal, C. Wolverton, Physical factors controlling the observed high-strength precipitate morphology in Mg-rare earth alloys, Acta Mater 65 (2014) 240–250.
[34] H. Kimizuka, S. Ogata, Predicting atomic arrangement of solute clusters in dilute Mg alloys, Mater. Res. Lett. 1 (2013) 213–219.
[35] T.W. Fan, B.Y. Tang, L.M. Peng, W.J. Ding, First-principles study of long-period stacking ordered-like multi-stacking fault structures in pure magnesium, Scr. Mater. 64 (2011) 942–945.
[36] S. Amelinckx, Dislocations in particular structures, in: F.R.N. Nabarro (Ed.), Dislocations in Solids, North-Holland, Amsterdam, 1979, p. 67.
[37] J.P. Hirth, J. Lothe, Theory of Dislocations, John Wiley & Sons, 1982.
[38] T.J. Jang, W.S. Choi, D.W. Kim, G. Choi, H. Jun, A. Ferrari, F. Kormann, P.P. Choi, S.S. Sohn, Shear band-driven precipitate dispersion for ultrastrong ductile medium-entropy alloys, Nat. Commun. 12 (2021) 4703.
[39] A.A. Nayeb-Hashemi, J.B. Clark, A. International, Phase Diagrams of Binary Magnesium Alloys, ASM International, 1988.
[40] M. Asta, R. Mccormack, D. Defontaine, Theoretical-study of alloy phase-stability in the Cd-Mg system, Phys. Rev. B 48 (1993) 748–766.
[41] Y.G. Zhang, W. Liu, J.S. Zhang, W. Zhu, Q.Q. Ma, X.M. Zong, C.X. Xu, Influence of micro-alloying with Cd on growth pattern, mechanical properties and microstructure of as-cast $Mg_{94}Y_{2.5}Zn_{2.5}Mn_1$ alloy containing LPSO structure, Mat. Sci. Eng. A-Struct. 748 (2019) 294–300.
[42] V.I. Bondarev, E.V. Ekhina, T.M. Kunyavskaya, T.M. Moskovchenko, An investigation of Bars of an Mg-Y-Cd system alloy after a strengthening heat-treatment, Met. Sci. Heat Treat. 30 (1988) 691–694.
[43] L. Elen, B. Cicek, E. Koc, Y. Turen, Y. Sun, H. Ahlatci, Effects of alloying element and cooling rate on properties of AM60 Mg alloy, Mater. Res. Express. 6 (2019) 096511.
[44] S.N. Xu, M.E. Ikpi, J.H. Dong, J. Wei, W. Ke, N. Chen, Effects of Cadmium alloying on the Corrosion and Mechanical Properties of Magnesium, Int. J. Electrochem. Sci. 7 (2012) 4735–4755.
[45] K. Gusieva, C.H.J. Davies, J.R. Scully, N. Birbilis, Corrosion of magnesium alloys: the role of alloying, Int. Mater. Rev. 60 (2014) 169–194.

[46] H. Xie, W. Lou, X. Zhao, S. Li, H. Pan, N. Xiao, H. Li, J. Bai, Y. Ren, G. Qin, Enhanced age-hardening response of the Mg-Sm alloy via alloying with Cd, Mater. Charact. 170 (2020) 110669.
[47] P. Villars, L. Calvert, L.D. Calvert, A.S.F. Metals, Pearson's Handbook of Crystallographic Data For Intermetallic Phases (Volumes 1-3), American Society for Metals1985.
[48] H.B. Xie, H.C. Pan, Y.P. Ren, S.N. Sun, L.Q. Wang, Y.F. He, G.W. Qin, Co-existences of the two types of β' precipitations in peak-aged Mg-Gd binary alloy, J. Alloy. Compd. 738 (2018) 32–36.
[49] S.X. Wang, Y. Zhang, L.M. Peng, On the evolution of β' precipitate during creep in a Mg-3.3Y-0.1Zr (at.%) alloy, Mater. Charact. 147 (2019) 414–420.
[50] J. Tan, Y. Dong, H.X. Zhang, Y.H. Sun, B.Z. Sun, Y. Qi, A new insight into the β''' structure: three categories of configurations between β' precipitates in aged binary Mg-Nd alloy, Scr. Mater. 172 (2019) 130–134.
[51] H. Liu, W.F. Xu, N.C. Wilson, L.M. Peng, J.F. Nie, Formation of and interaction between β_F' and β' phases in a Mg-Gd alloy, J. Alloy. Compd. 712 (2017) 334–344.
[52] H. Liu, W.F. Xu, L.M. Peng, W.J. Ding, J.F. Nie, A simulation study of the distribution of β' precipitates in a crept Mg-Gd-Zr alloy, Comp. Mater. Sci. 130 (2017) 152–164.
[53] C.H. Peng, D.J. Li, X.Q. Zeng, W.J. Ding, First principles investigation of β'-short and β'-long in Mg-Gd alloy, J. Alloy. Compd. 671 (2016) 177–183.
[54] W.F. Xu, Y. Zhang, L.M. Peng, W.J. Ding, J.F. Nie, Linear precipitate chains in Mg-2.4Gd-0.1Zr alloy after creep, Mater. Lett. 137 (2014) 417–420.
[55] M. Nishijima, K. Hiraga, M. Yamasaki, Y. Kawamura, Characterization of β' phase precipitates in an Mg-5 at% Gd alloy aged in a peak hardness condition, studied by high-angle annular detector dark–field scanning transmission electron microscopy, Mater. Trans. 47 (2006) 2109–2112.
[56] H.W. Chen, C.L. Liu, Z.Q. Li, P. Li, A.P. Zhang, J.F. Nie, Effect of Ca addition on microstructures of aged Mg-15Gd-0.5Zr alloy, Mater. Charact. 156 (2019).
[57] A. Sanaty-Zadeh, A.A. Luo, D.S. Stone, Comprehensive study of phase transformation in age-hardening of Mg-3Nd-0.2Zn by means of scanning transmission electron microscopy, Acta Mater 94 (2015) 294–306.
[58] K. Saito, H. Kaneki, TEM study of real precipitation behavior of an Mg-0.5at%Ce age-hardened alloy, J. Alloy. Compd. 574 (2013) 283–289.
[59] K. Saito, A. Yasuhara, M. Nishijima, K. Hiraga, Structural changes of precipitates by aging of an Mg-4 at%Dy solid solution studied by atomic-scaled transmission electron microscopy, Mater. Trans. 52 (2011) 1009–1015.
[60] X. Gao, S.M. He, X.Q. Zeng, L.M. Peng, W.J. Ding, J.F. Nie, Microstructure evolution in a Mg-15Gd-0.5Zr (wt.%) alloy during isothermal aging at 250 ^{o}C, Mat. Sci. Eng. A-Struct. 431 (2006) 322–327.
[61] P.J. Apps, H. Karimzadeh, J.F. King, G.W. Lorimer, Precipitation reactions in magnesium-rare earth alloys containing Yttrium, Gadolinium or Dysprosium, Scr. Mater. 48 (2003) 1023–1028.